Wave Motion 51 (2014) 1021–1043

Contents lists available at ScienceDirect

Wave Motion

journal homepage: www.elsevier.com/locate/wavemoti

Acoustic wave propagation in inhomogeneous, layered waveguides based on modal expansions and hp-FEM

K.A. Belibassakis [a,*], G.A. Athanassoulis [a], T.K. Papathanasiou [b], S.P. Filopoulos [b], S. Markolefas [b]

[a] School of Naval Architecture and Marine Engineering, National Technical University of Athens, Zografos 15773, Athens, Greece
[b] School of Applied Mathematical and Physical Science, National Technical University of Athens, Zografos 15773, Athens, Greece

HIGHLIGHTS

- Coupled-mode model for propagation/scattering in inhomogeneous, layered waveguides.
- Modal expansion enhanced by additional terms for sloping boundaries and interfaces.
- hp-FEM for local vertical eigenvalue problems and the horizontal coupled mode system.
- Simulations showing the role of additional modes and the convergence of the method.
- The method can be naturally extended to efficiently treat stratified 3D waveguides.

ARTICLE INFO

Article history:
Received 6 November 2013
Received in revised form 24 March 2014
Accepted 6 April 2014
Available online 18 April 2014

Keywords:
Inhomogeneous acoustic waveguides
Layered medium
Coupled modes
Finite elements

ABSTRACT

A new model is presented for harmonic wave propagation and scattering problems in non-uniform, stratified waveguides, governed by the Helmholtz equation. The method is based on a modal expansion, obtained by utilizing cross-section basis defined through the solution of vertical eigenvalue problems along the waveguide. The latter local basis is enhanced by including additional modes accounting for the effects of inhomogeneous boundaries and/or interfaces. The additional modes provide implicit summation of the slowly convergent part of the local-mode series, rendering the remaining part to be fast convergent, increasing the efficiency of the method, especially in long-range propagation applications. Using the enhanced representation, in conjunction with an energy-type variational principle, a coupled-mode system of equations is derived for the determination of the unknown modal-amplitude functions. In the case of multilayered environments, *h*- and *p*-FEM have been applied for the solution of both the local vertical eigenvalue problems and the resulting coupled mode system, exhibiting robustness and good rates of convergence. Numerical examples are presented in simple acoustic propagation problems, illustrating the role and significance of the additional mode(s) and the efficiency of the present model, that can be naturally extended to treat propagation and scattering problems in more complex 3D waveguides.

© 2014 Elsevier B.V. All rights reserved.

1. Introduction

Acoustic propagation in inhomogeneous, layered waveguides is an interesting problem finding important applications, as, e.g., underwater acoustic propagation and scattering in shallow water and seismoacoustics [1–3], atmospheric acoustics

* Corresponding author. Tel.: +30 210 7721138; fax: +30 210 7721397.
E-mail address: kbel@fluid.mech.ntua.gr (K.A. Belibassakis).

http://dx.doi.org/10.1016/j.wavemoti.2014.04.002
0165-2125/© 2014 Elsevier B.V. All rights reserved.

[4] and other. Similar problems governed by the Helmholtz equation are also encountered in variable cross-section electromagnetic waveguides; see e.g., Ref. [5]. Several methods for treating this, generally non-separable, boundary value problem have been developed, ranging from fully numerical, finite element and finite difference methods, to semi-analytical ones, like wavenumber integration, boundary integral equation and coupled-mode techniques, as well as various asymptotic models, like ray theory and the adiabatic and parabolic approximations; see [3,6]. Also, meshless methods have been developed; see, e.g., [7,8] and the references cited therein. Fully numerical methods, are computationally intense and thus, their use is more appropriate for short-range/low-frequency propagation and local scattering problems. These methods have been proved very useful, in the case of general ocean-acoustic propagation problems, for providing benchmark solutions. The problem becomes more demanding in (partially) infinite waveguides excited by high-frequency requiring special treatment (e.g., [9,10]). Boundary element methods are more suitable in the case of a homogeneous medium (e.g., [11]), but they become less practical in the presence of inhomogeneities of the acoustic parameters, due to the difficulties associated with the calculation of Green's function.

In environments with steep interface boundaries, large bottom slopes and/or media with variable index of refraction the method of coupled modes [12,13] has been developed to treat the problem, by subdividing the waveguide into a finite number of adjacent columns of different depth where the speed of sound exhibits vertical variation. The wave field is represented as a normal-mode series based on vertical eigenfunctions within each one of the elements, and the coefficients are obtained by matching the expansions on the inter-element vertical interfaces. The main feature of this model is the full coupling between the modes and the representation of the backscattering effect. However, the approximation of continuous distributions of acoustic parameters by horizontally piecewise constant functions may require a large number of steps, in order that the horizontal stair-step size to be small enough for avoid strong numerical backscattering, [14,15]. Besides, the stepwise approximation of the bottom renders the numerical solution procedure cumbersome in the vicinity of a continuously varying bottom boundary. Another approach for treating the non-homogeneous waveguide in the context of coupled-mode theory is based on local mode expansions; see, e.g., [1,16]. Thus, the problem is reformulated equivalently a coupled system of differential equation on the horizontal plane offering reduction of dimensionality at the cost of increase of unknowns which are now the horizontal mode amplitudes. However, in the case of non-homogeneous waveguides the local-mode series may exhibit slow convergence, as discussed in Ref. [17].

In this work, a fast-convergent model based on modal expansions and FEM is presented for treating harmonic wave propagation and scattering problems in stratified, non uniform waveguides, governed by the Helmholtz equation. The method is based on a local mode series expansion, obtained by utilizing local eigenfunction systems defined through the solution of corresponding eigenvalue problems, formulated along the cross section of the waveguide. In the works by Athanassoulis & Belibassakis [18] and Athanassoulis et al. [19] the local mode series is enhanced by including additional modes accounting for the effects of inhomogeneous waveguide boundaries and/or interfaces. The additional modes provide an implicit summation of the slowly convergent part of the local-mode series, rendering the remaining part to be fast convergent, and substantially increasing the efficiency of the method, especially in long-range applications; see also Athanassoulis & Belibassakis [20], Hazard & Lunéville [21] and Mercier & Maurel [22]. Using the enhanced local mode expansion, in conjunction with an energy-type variational principle, a coupled-mode system of equations is derived for the determination of the unknown modal-amplitude functions.

The enhanced local-mode series includes an additional mode for each interface in the layered waveguide enabling the consistent satisfaction of the corresponding condition on the non-horizontal parts of the interface and providing rapid mode convergence and ensuring energy conservation in the case of a lossless acoustic waveguide. The improved coupled-mode system is derived by means of an appropriate variational principle and is fully equivalent to the boundary value problem. We note here that the concept of the additional mode has been first introduced and studied by the authors in the context of small-amplitude water waves propagating over variable bathymetry regions [18,23,24]. This approach has been extended to non-linear water waves [25,26] and hydrodynamic interaction problems with floating rigid and elastic bodies [27,28].

In all previous works the resulting coupled mode system of differential equations on the horizontal plane (propagation space) is numerically treated by a second-order finite difference scheme based on uniform grid. Although the present reformulation has been proved quite more efficient in comparison with direct numerical solvers of the problem applied in the initial multidimensional domain, still the present approach remains very demanding especially for long range and high frequency applications, where the computational requirements increase substantially. An option of further improvement from the point of view of computational cost and efficiency is offered by implementing *h*- and *p*-Finite Element Methods (see, e.g., Hughes [29]) for the numerical solution of both the local vertical eigenvalue problems (VEP), as well as for the solution of the resulting coupled-mode system. On the basis of the former solution of the VEP, the coefficients of the coupled-mode system are efficiently calculated in the general case of multilayered waveguide by numerical integration. Subsequently, the solution of the present coupled-mode system is obtained by repetitive application of *h*- and *p*-FEM, based on general mesh, offering good rates of convergence and adaptivity option for mesh refinement.

The present work is structured as follows: In Section 2 the mathematical formulation of the problem is presented. The waveguide is treated by applying domain decomposition separating the physical domain into a bounded, inhomogeneous middle part connecting two homogeneous semi-infinite subdomains. Using appropriate normal-mode expansions for the representation of the wave field in the two semi-infinite regions of incidence and transmission, respectively, the problem is equivalently reformulated in the form of a variational principle in the bounded subdomain containing the irregularity. Next, in Section 3 the local mode series expansion for the representation of the wave field in the inhomogeneous subregion

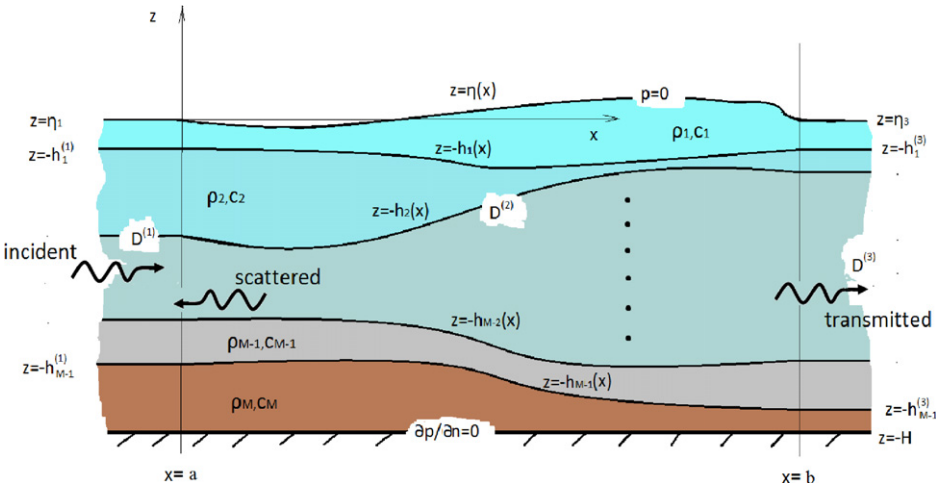

Fig. 1. Multilayered two-dimensional acoustic waveguide.

is presented. This expansion contains, except of the standard local vertical modes generated by the VEP, also additional terms associated with each variable interface. The latter terms enable the consistent satisfaction of the corresponding conditions and increase the rate of convergence of the series, permitting its truncation keeping only its first terms. Substituting the above representations in the variational principle the coupled-mode system is derived on the horizontal plane. Subsequently, in Section 4, the application of *h*- and *p*-Finite Element Methods is presented and discussed for the numerical solution of the local VEP, at each horizontal position. The behavior of the numerical solution is examined in comparison with known analytical solutions showing that it converges rapidly, and verifying the theoretical results concerning error estimation. Then, in Section 5 the *h*- and *p*-FEM is presented and discussed for the numerical solution of the resulting coupled mode system, in the case of general, multilayered waveguides, including detailed investigation of the error and showing the achieved rate of convergence in conformity with theoretical predictions. Finally, in Section 5, specific numerical examples are presented illustrating the applicability of the present numerical model in cases of higher frequency and multilayered environments, and furthermore demonstrating the overall efficiency of the present method, that can be naturally extended to treat similar propagation and scattering problems in more complicated 3D waveguides.

2. Formulation of the problem

We consider the multilayered waveguide of Fig. 1 with general interfaces separating the layers. For simplicity we restrict ourselves to a 2D problem in an ocean acoustic environment, governed by the Helmholtz equation. However, the present method and analysis can be naturally extended to treat more general 3D acoustic waveguides and similar wave propagation problems.

The domain $D = D^{(1)} \cup D^{(2)} \cup D^{(3)}$ is decomposed into three parts $D^{(m)}$, $m = 1, 2, 3$ (see Fig. 1), as follows: $D^{(1)}$ is the subdomain characterized by $x < a$ where the cross (vertical) dimension is constant and equal to $H^{(1)} = H + \eta_1$, and $D^{(3)}$ is the subdomain characterized by $x > b\,(b > a)$, where the cross dimension is constant and equal to $H^{(3)} = H + \eta_3$. Thus, $D^{(2)}$ is the variable cross section subdomain lying between $D^{(1)}$ and $D^{(3)}$. A similar decomposition is also applied to the (upper and lower) boundaries, as well as to the internal interfaces.

The acoustic medium inside the domain is stratified. The sound speed (c) and density (ρ) in the layers vary with respect to the both (x, z) coordinates in the middle range-dependent subdomain $D^{(2)}$, and present only vertical variability in the two semi-infinite subdomains $D^{(1)}$ and $D^{(3)}$. Assuming that the whole domain consists of M layers, a total number of $M - 1$ interfaces at $z = -h_j(x), j = 1, 2, \ldots, M-1$, are considered, where $h_j(x)$ denotes the local depth of each interface measured from the upper (still water) level; see Fig. 1. Thus, $D^{(\ell)} = \bigcup_{j=1,M} D_j^{(\ell)}$, $\ell = 1, 2, 3$.

The waveguide is terminated below by a perfectly rigid (acoustically hard) horizontal boundary, located at $z = -h_M = -H$. On the other hand, the waveguide is terminated above by an acoustically soft boundary, located at $z = \eta\,(x) = -h_0\,(x)$. For ocean acoustic applications, the latter boundary models the free surface which may deviate from the horizontal calm-water position, if we consider effects by tidal and large-scale flows that present very slow variability in space and in time (with respect to the wave propagation speed). Thus, similarly as the internal interfaces, the above boundary can be treated as fixed, stationary surface, which is justified for time intervals corresponding to many cycles of the acoustic wave motion.

The density $\rho_j, j = 1, 2, \ldots, M$, is assumed to be constant within each layer, presenting possibly sharp discontinuities at the interfaces. Moreover, the sound speed $c_j\,(x, z), j = 1, 2, \ldots, M$, presents both vertical and horizontal variability in the middle subdomain $D^{(2)}$, and could also exhibit strong discontinuity at the interfaces. The sound speed becomes function only of z in the two semi-infinite subdomains $D^{(1)}$ and $D^{(3)}$, which are then range independent subdomains with respect to

both geometry and physical parameters. This assumption permits us to obtain complete normal-mode expansions of the wave field in the above semi-infinite regions by means of separation of variables, and consistently formulate the conditions of wave incidence and reflection at the entrance of the variable part of the waveguide ($x = a$) and wave transmission at the exit ($x = b$), respectively.

2.1. Governing equation, boundary and interface conditions

Restricting ourselves to monochromatic waves of angular frequency $\omega = 2\pi f$, the acoustic harmonic wave propagation problem inside the multi-layered waveguide is governed by the Helmholtz equation.

The boundary value problem (see [1–3]) consists of finding the continuous function $p(x, z)$ representing the complex amplitude of the acoustic pressure ($p(x, z; t) = \mathrm{Re}\{p(x, z)e^{-i\omega t}\}$) such that

$$\nabla \cdot \left(\frac{1}{\rho}\nabla p\right) + \frac{k^2}{\rho}p = 0, \quad \text{in } D, \tag{1}$$

where the wavenumber $k(x, z) = \omega/c(x, z)$ is a piecewise smooth function of the spatial coordinates, presenting discontinuities $z = -h_j(x), j = 1, 2, \ldots, M-1$. Moreover, Eq. (1) is supplemented by the following boundary conditions

$$p = 0, \quad \text{on } z = \eta(x), \tag{2a}$$

$$\partial p/\partial n = 0, \quad \text{on } z = -H, \tag{2b}$$

and the interface conditions

$$\frac{1}{\rho_j}\frac{\partial p}{\partial n} = \frac{1}{\rho_{j+1}}\frac{\partial p}{\partial n} \quad \text{on } z = -h_j(x),\ j = 1, 2, \ldots, M-1. \tag{3}$$

In the above equations $\partial p/\partial n = \mathbf{n}\nabla p$ denotes the normal derivative, where $\mathbf{n}$ is the unit normal vector on each boundary and interface. We consider a transmission problem forced by waves propagating in the positive x direction. The waves are incident from $D^{(1)}$, and then they are refracted and scattered in the range dependent subdomain $D^{(2)}$, and finally transmitted in $D^{(3)}$.

Except of the effects and the treatment of various inhomogeneities, a significant difficulty in the numerical solution of the above problem is encountered in long-range and high-frequency applications, where the non-dimensional wavenumber $\kappa = \max\{k_*(b-a), k_*H\}$ increases ($\kappa \gg 1$), with k_* denoting a characteristic (e.g. mean or max) value of $k(x, z)$ in the domain.

In the present work it is assumed that the boundaries and interfaces of the acoustic waveguide are non intersecting. Denoting by $h_0(x) = -\eta(x)$ and by $h_M(x) = H$, the above restriction is satisfied by requiring $h_j(x) > h_{j+1}(x)$, for all $j = 0, 1, 2, \ldots, M-1$. In the special case of intersecting interfaces the calculation of the acoustic field presents difficulties that could be treated by considering the part between local intersection points as an inclusion; see, e.g., the recent work by Maurel et al. [30]. Furthermore, in order to treat the present problem in the infinite domain, complete normal-mode type representations of the wave field in the regions of incidence $D^{(1)}$ and transmission $D^{(3)}$ are derived by separation of variables. In particular, the expansion of the wavefield in $D^{(1)}$ consists of incident and reflected (scattered) waves is as follows,

$$p^{(1)}(x, z) = \sum_{n=1}^{\infty}\left(A_n^{(1)}\exp\left(ik_n^{(1)}x\right) + B_n^{(1)}\exp\left(-ik_n^{(1)}x\right)\right)Z_n^{(1)}(z), \tag{4}$$

where the functions $Z_n^{(1)}(z)$ and the numbers $k_n^{(1)}$, $n = 1, 2, 3, \ldots$, satisfy the following vertical eigenvalue problem in $D^{(1)}$

$$\frac{d^2Z_n^{(1)}}{dz^2} + \left[\left(k^{(1)}(z)\right)^2 - (k_n^{(1)})^2\right]Z_n^{(1)} = 0, \tag{5}$$

$$Z_n^{(1)}(z = \eta_1) = 0, \tag{6a}$$

$$\frac{dZ_n^{(1)}(z = -H)}{dz} = 0, \tag{6b}$$

$$Z_n^{(1)}(-h_j^{(1)} + 0) = Z_n^{(1)}(-h_j^{(1)} - 0), \quad j = 1, 2, M-1, \tag{6c}$$

and

$$\frac{1}{\rho_j}\frac{\partial Z_n^{(1)}(-h_j^{(1)} + 0)}{\partial z} = \frac{1}{\rho_{j+1}}\frac{Z_n^{(1)}(-h_j^{(1)} - 0)}{\partial z}, \quad j = 1, 2, M-1, \tag{6d}$$

where $k^{(1)}(z) = \omega/c^{(1)}(z)$; see also [2,3]. Similarly, the expansion of the acoustic wavefield in the region of transmission $D^{(3)}$, consists only of outgoing transmitted waves, and is given by

$$p^{(3)}(x,z) = \sum_{n=1}^{\infty} A_n^{(3)} \exp\left(ik_n^{(3)}x\right) Z_n^{(3)}(z), \tag{7}$$

where the eigenfunctions $Z_n^{(3)}(z)$ and the corresponding eigenvalues $k_n^{(3)}$, $n = 1, 2, 3, \ldots$, are obtained by similar vertical eigenvalue problems formulated in $D^{(3)}$. From the properties of Sturm–Liouville problems [31,32], the eigenvalues $\{(k_n^{(m)})^2, n = 1, 2, \ldots\}$, $m = 1, 3$, are discrete, infinite, with continuously decreasing moduli, and thus, the corresponding parameters $\{k_n^{(m)}, n = 1, 2, 3, \ldots\}$, are subdivided into a finite real subset $\{k_n^{(m)}, n = 1, 2, 3, \ldots, N_p^{(m)}\}$ and an infinite imaginary one $\{i|k_n^{(m)}|, n = N_p^{(m)} + 1, \ldots\}$, where $N_p^{(m)}$, denotes the number of propagating modes in $D^{(m)}$, $m = 1, 3$, which is dependent on the physical parameters in these subregions and increases with frequency. Clearly, in order for the wave field to remain bounded at infinity, the coefficients of the expansion $A_n^{(1)} = 0$, $n > N_p^{(1)}$, and thus, Eq. (4) takes the form

$$p^{(1)}(x,z) = \sum_{n=1}^{N_p^{(1)}} A_n^{(1)} \exp\left(ik_n^{(1)}x\right) Z_n^{(1)}(z) + \sum_{n=1}^{\infty} B_n^{(1)} \exp\left(-ik_n^{(1)}x\right) Z_n^{(1)}(z). \tag{8}$$

Moreover, the terms $\exp(-ik_n^{(1)}x)Z_n^{(1)}(z)$, $n > N_p^{(1)}$, and $\exp(ik_n^{(3)}x)Z_n^{(3)}(z)$, $n > N_p^{(3)}$, are the evanescent modes in $D^{(m)}$, $m = 1, 3$, respectively. These modes decay exponentially at large distances from the inhomogeneity in the two semi-infinite strips.

2.2. Mode excitation of the waveguide

The complex coefficients $A_n^{(1)}$ of the modes $A_n^{(1)} \exp(ik_n^{(1)}x)Z_n^{(1)}(z)$, $n \le N_p^{(1)}$, constitute the given data associated the specification of the incident wave field in $D^{(1)}$. Due to the linearity of the problem each one of the above modes could be separately considered as forcing of the present acoustic waveguide and the general solution is obtained by superposition of the corresponding responses. Thus, if we denote the waveguide response to unit modal forcing by $p_{(n)}(x,z) = p(x,z; A_n^{(1)} = 1)$, the general solution of the examined problem is expressed by

$$p(x,z) = \sum_{n=1}^{N_p^{(1)}} A_n^{(1)} p_{(n)}(x,z). \tag{9}$$

The above formulation can also be exploited to treat scattering of acoustic waves emitted by a line source (see, e.g., [3,33,34]), located in the region of incidence at $(x_S, z_S) \in D^{(1)}$ far from the inhomogeneity ($x_S \ll a$). In fact, by using the modal expansion of the 2D Green's function in the homogeneous subdomain $D^{(1)}$ (see, e.g., Jensen et al. [3], Sec.5.2.2)

$$G(x,z;x_S,z_S) = \frac{i}{2\rho(z_S)} \sum_{n=1}^{N_p^{(1)}} \frac{Z_n^{(1)}(z_S)}{k_n^{(1)}} \exp\left(ik_n^{(1)}x\right), \quad a > x \gg x_S, \tag{10a}$$

we obtain the following expression in the general solution of the acoustic field emitted by the line source in the inhomogeneous waveguide in terms of the mode responses $p_{(n)}(x,z)$

$$p_G(x,z;x_S,z_S) = \frac{i}{2\rho(z_S)} \sum_{n=1}^{N_p^{(1)}} \frac{Z_n^{(1)}(z_S)}{k_n^{(1)}} p_{(n)}(x,z). \tag{10b}$$

On the basis of the above considerations and for simplicity in the presentation we shall use the same notation $p(x,z)$ for the solution of the problem corresponding to each mode response of the inhomogeneous waveguide or any combination of them.

2.3. Variational formulation

By exploiting the representations (7) and (8), the problem can be formulated as a transmission boundary value problem in the bounded subdomain $D^{(2)}$, satisfying Eqs. (1)–(3) and the following matching conditions:

$$p^{(2)}(x,z) = p^{(1)}(x,z), \qquad \frac{\partial p^{(2)}}{\partial x} = \frac{\partial p^{(1)}}{\partial x}, \quad x = a, \ -H < z < \eta_1, \tag{11a}$$

$$p^{(2)}(x,z) = p^{(3)}(x,z), \qquad \frac{\partial p^{(2)}}{\partial x} = \frac{\partial p^{(3)}}{\partial x}, \quad x = b, \ -H < z < \eta_3. \tag{11b}$$

We proceed to formulate a functional $\mathcal{F}$ allowing us to state a variational formulation of the transmission problem. The admissible function space for the wave field in the inhomogeneous subregion $p^{(2)}(x,z) \in D^{(2)}$ (that is also simply denoted from now on as p), consists of globally continuous and piecewise smooth functions, possessing continuous second derivatives in the interior of each layer, such that

$$p(x, z=\eta(x)) = 0 \quad \text{and} \quad \frac{\partial p(x, z=-H)}{\partial n} = \frac{\partial p(x, z=-H)}{\partial z} = 0. \tag{12}$$

For this purpose, we consider the following energy-type functional on the acoustic field in the bounded subdomain and on the unknown coefficients of the expansions in the regions of incidence and transmission,

$$\begin{aligned}\mathcal{F}\left(p, \left\{B_n^{(1)}\right\}, \left\{A_n^{(3)}\right\}\right) = \frac{1}{2}\sum_{j=1}^{M}\Bigg\{ & \frac{1}{\rho_j}\int_{D_j^{(2)}}\left[(\nabla p)^2 - k^2(p)^2\right] dxdz \\ & + \int_{z=-h_{j+1}(a)}^{z=-h_j(a)}\left(p - \frac{1}{2}p^{(1)}\left(\left\{B_n^{(1)}\right\}\right)\right)\frac{\partial p^{(1)}\left(\left\{B_n^{(1)}\right\}\right)}{\partial x}dz \\ & - \int_{z=-h_{j+1}(b)}^{z=-h_j(b)}\left(p - \frac{1}{2}p^{(3)}\left(\left\{A_n^{(3)}\right\}\right)\right)\frac{\partial p^{(3)}\left(\left\{A_n^{(3)}\right\}\right)}{\partial x}dz\Bigg\}.\end{aligned} \tag{13}$$

The present problem admits of an equivalent variational formulation which is expressed by the stationarity of the above functional

$$\delta\mathcal{F}\left(p; \left\{B_n^{(1)}\right\}, \left\{A_n^{(3)}\right\}\right) = 0. \tag{14}$$

Using Green's theorem in conjunction with Eq. (12), the above variational equation takes the form

$$\begin{aligned}\sum_{j=1}^{M}\frac{1}{\rho_j}\Bigg\{ & -\int_{D_j^{(2)}}\left(\nabla^2 p + k_j^2 p\right)\delta p\, dxdz - \sum_{j=1}^{M-1}\int_{x=a}^{x=b}\left(\frac{1}{\rho_j}\frac{\partial p}{\partial N} - \frac{1}{\rho_{j+1}}\frac{\partial p}{\partial N}\right)_{z=-h_j(x)}\delta p\, dx \\ & + \frac{1}{\rho_1}\int_{x=a}^{x=b}\left(\frac{\partial p}{\partial z} + \frac{d\eta}{dx}\frac{\partial p}{\partial x}\right)_{z=\eta}\delta p\, dx - \int_{z=-h_{j+1}(a)}^{z=-h_j(a)}\left(\frac{\partial p}{\partial x} - \frac{\partial p^{(1)}}{\partial x}\right)_{x=a}\delta p\, dz \\ & - \int_{z=-h_{j+1}(b)}^{z=-h_j(b)}\left(\frac{\partial p}{\partial x} - \frac{\partial p^{(3)}}{\partial x}\right)_{x=b}\delta p\, dz - \int_{z=-h_{j+1}(b)}^{z=-h_j(b)}\left(p - p^{(3)}\right)_{x=b}\delta\frac{\partial p^{(3)}}{\partial x}dz \\ & + \int_{z=-h_{j+1}(a)}^{z=-h_j(a)}\left(p - p^{(1)}\right)_{x=a}\delta\frac{\partial p^{(1)}}{\partial x}dz\Bigg\} = 0,\end{aligned} \tag{15}$$

where $\frac{\partial p}{\partial N}\big|_{z=-h_j(x)} = \frac{\partial p}{\partial z} + \frac{dh_j}{dx}\frac{\partial p}{\partial x} = \frac{\partial p}{\partial n}\left(1 + \left(dh_j/dx\right)^2\right)^{1/2}$.

The usefulness of the above variational principle hinges on the fact that it leaves us the freedom to choose any particular representation for the unknown field $p(x,z) \in D^{(2)}$. In this way, a variety of possible algorithms for the numerical solution of the present wave problem can be constructed.

3. Derivation of the coupled mode system

One possible choice, facilitating the treatment of studied wave problems in general waveguides, without restrictions as regards the slope and/or curvature of the interfaces and the variation of physical parameters, will be presented in the following section.

3.1. Enhanced local-mode representation of the acoustic field in the inhomogeneous subdomain

Inside the bounded domain $D^{(2)}$, a spectral-type representation of the acoustic field $p(x,z)$ is used in the present work, which based on the following local-mode series,

$$p(x,z) = \sum_{n=1}^{\infty} U_n(x) Z_n(z;x), \tag{16}$$

where $U_n(x)$ are complex coefficients depending on the horizontal position. The family of real functions $Z_n(z;x)$ appearing in the above spectral-type expansion, is parametrically dependent on x and is obtained by formulating and solving local,

vertical Sturm–Liouville problems, of the form of Eqs. (5), (6), formulated in the z-intervals $[-H,\ \eta(x)]$, for each horizontal position $a < x < b$, as follows

$$\frac{d^2Z_n}{dz^2} + \left[\left(k^{(1)}(z;x)\right)^2 - (k_n^{(1)})^2\right] Z_n^{(1)} = 0, \tag{17}$$

$$Z_n(z = \eta(x)) = 0, \tag{18a}$$

$$\frac{dZ_n(z=-H)}{dz} = 0, \tag{18b}$$

$$Z_n(-h_j(x)+0) = Z_n(-h_j(x)-0), \quad j = 1, 2,\ M-1, \tag{18c}$$

$$\frac{1}{\rho_j}\frac{\partial Z_n(-h_j(x)+0)}{\partial z} = \frac{1}{\rho_{j+1}}\frac{Z_n(-h_j(x)-0)}{\partial z}, \quad j = 1, 2,\ M-1. \tag{18d}$$

Based on the properties of the local vertical eigenfunctions, the above representation (16) becomes a basis in the admissible function space. However, any finite truncation of the series (16) is incompatible with the sloping interface conditions, Eqs. (3), whenever $dh_j(x)/dx \neq 0, j = 1, 2, \ldots, M-1$, rendering the above series to converge only in an L^2-sense, and the coefficients U_n to present a slow decay of the order $O(n^{-2})$, where n is the mode number. This fact has been discussed in detail in the case of similar problems governed by the Laplace equation concerning water waves propagating in variable bathymetry regions [18], where the concept of additional sloping bottom mode is introduced offering consistency in the formulation and substantially accelerating the convergence of the local mode series; see also Refs. [19–21].

To remedy the above inconsistency in the present multilayered environment, an additional mode associated with each interface is introduced, and denoted by $U_n(x)Z_n(z;x)$, $n = -M+2, \ldots, -1, 0$. These additional terms are called the sloping-interface modes. Thus, we obtain the following enhanced local-mode series

$$p(x,z) = \sum_{n=-M+2}^{0} U_n(x)Z_n(z;x) + \sum_{n=1} U_n(x)Z_n(z;x). \tag{19}$$

For every horizontal position $a < x < b$, the vertical structure of the sloping-interface modes $Z_n(z;x)$ corresponding to the first sum in the right-hand side of the above equation (with non-positive index), is any globally continuous and piecewise smooth function defined with support only in the local vertical intervals $z \in [-h_{j+1}(x), -h_j(x)]$, $j = -n$, $n = -M+2, \ldots, -1, 0$, respectively, satisfying the following jump condition(s) concerning the vertical derivative at $z = -h_{j+1}(x)$,

$$\frac{1}{\rho_{j+1}}\frac{\partial Z_n}{\partial z}\bigg|_{z=-h_{j+1}^+} - \frac{1}{\rho_{j+2}}\frac{\partial Z_n}{\partial z}\bigg|_{z=-h_{j+1}^-} = \frac{1}{\rho_{j+1}}\frac{\partial Z_n\left(z=-h_{j+1}(x)+0\right)}{\partial z} = 1, \quad j = -n = 0, 1, 2, \ldots, M-2. \tag{20a}$$

Moreover, the function $Z_0(z;x)$ should satisfy the homogeneous Dirichlet condition at $z = \eta(x) = -h_0(x)$. Using the fact that non intersecting interfaces/boundaries have been considered for the present acoustic waveguide (i.e., $h_j(x) > h_{j+1}(x)$, $j = 0, 1, 2, \ldots, M-1$), a convenient choice based on the low degree polynomial satisfying the above conditions is

$$Z_n(z;x) = -\rho_{j+1}\left(h_{j+1}(x) - h_j(x)\right)\left(\left(\frac{z+h_j(x)}{h_{j+1}(x)-h_j(x)}\right)^4 + \left(\frac{z+h_j(x)}{h_{j+1}(x)-h_j(x)}\right)^3\right), \tag{20b}$$

in $-h_{j+1}(x) \le z \le -h_j(x)$ and zero elsewhere.

Using Eqs. (18d) and (20) in the enhanced representation, Eq. (19), we find that the amplitude of the additional modes satisfies

$$U_n(x) = \frac{1}{\rho_{j+1}}\frac{\partial p}{\partial z}\bigg|_{z=-h_{j+1}^+} - \frac{1}{\rho_{j+2}}\frac{\partial p}{\partial z}\bigg|_{z=-h_{j+1}^-}, \quad j = -n = 0, 1, 2, \ldots, M-2. \tag{21}$$

Consequently, the $M-1$ terms $U_n(x)Z_n(z;x)$, $n = 0, -1, -2, \ldots, -M+2$, appearing in the first series in the right-hand term of the enhanced representation given by Eq. (17) are the additional degrees of freedom in the bounded subdomain $D^{(2)}$, permitting the consistent satisfaction of interface conditions Eq. (3), involving the normal derivative. Also, we immediately see that in the homogeneous parts of the waveguide, where the interfaces become flat horizontal, the additional sloping interface modes become zero, $U_n(x) = 0$, $n = 0, -1, -2, \ldots, -M+2$, and the enhanced representation Eq. (19) automatically reduces to Eq. (16). Furthermore, it is clear from Eqs. (18a), (18b) and (21) that the present representation fulfills the Dirichlet and Neumann boundary conditions Eqs. (2a) and (2b), respectively, all over the inhomogeneous subdomain, and thus, it becomes a basis of the admissible function space to be used in the variational principle, Eq. (15).

An important effect of the additional sloping-interface modes is to significantly increase the rate of decay of modal amplitudes. As it will be demonstrated in the next section, the modes associated with the enhanced series exhibit a rapid

decay rate: $|U_n(x)| \leq C(x)n^{-4}, n \to \infty, \forall x \in [a, b]$. The bound $C(x)$ is a continuous function on $[a, b]$ and, thus, the previous estimate is global: $|U_n| = O(n^{-4})$. If the additional modes are not included, then the rate of decay of the modes in the series (16) is only $|U_n| = O(n^{-2})$. The additional modes provide an implicit summation of the slowly convergent part of the local-mode series, rendering the remaining part to be fast convergent, increasing the efficiency of the method, which is important especially for long-range and high-frequency propagation problems.

3.2. The coupled mode system on the horizontal plane

Having calculated the eigenfunctions and the extra vertical modes for all horizontal points in $a < x < b$, we proceed to the calculation of the respective modal amplitudes $\{U_n(x), n = -M+2, \ldots, -1, 0, 1, 2, \ldots\}$. Following a similar procedure as the one described in detail in Ref. [18], we substitute the enhanced local mode representation (19), in conjunction with the normal-mode representations Eqs. (7) and (8), in the variational principle (15), and express the variation of the unknown field $p(x, z) \in D^{(2)}$, through the variations of the modal amplitudes as follows $\delta p(x, z) = \sum_{n=-M+2} Z_n(z; x)\, \delta U_n(x)$.

Theorem 1. *By considering only the variations $\delta U_n(x)$, $n = -M+2, \ldots, 0, 1, \ldots$, associated with each mode, for points in $a < x < b$, we obtain from the first term in the left hand side of Eq. (15) the following coupled-mode system (CMS) of second-order ordinary differential equations, with respect to the mode amplitudes $U_n(x)$, $n = -M+2, \ldots, 0, 1, 2, \ldots$,*

$$\sum_{n=-M+2} a_{mn}(x) \frac{d^2 U_n(x)}{dx^2} + b_{mn}(x) \frac{dU_n(x)}{dx} + c_{mn}(x)\, U_n(x) = 0, \tag{22}$$

where $m = -M+2, \ldots, 0, 1, 2, \ldots$. The x-dependent coefficients a_{mn}, b_{mn} and c_{mn} are defined in terms of the local vertical functions $Z_n(z; x)$ in $a < x < b$ and are given by

$$a_{mn} = \langle Z_n, Z_m \rangle, \tag{23a}$$

$$b_{mn} = 2\left\langle \frac{\partial Z_n}{\partial x}, Z_m \right\rangle + \sum_{j=1}^{M-1} \left(\frac{1}{\rho_j} - \frac{1}{\rho_{j+1}} \right) \frac{dh_j}{dx} Z_n(-h_j) Z_m(-h_j), \tag{23b}$$

$$c_{mn} = \left\langle \frac{\partial^2 Z_n}{\partial x^2} + \frac{\partial^2 Z_n}{\partial z^2} + k^2 Z_n, Z_m \right\rangle + \sum_{j=1}^{M-1} \left([\![Z_{n,z}]\!] + \frac{dh_j}{dx} [\![Z_{n,x}]\!] \right) Z_m(-h_j) \tag{23c}$$

In the above relations $\langle f, g \rangle := \int_{-H}^{\eta} \rho^{-1} f(z) g(z) dz$ denotes the weighted inner product in $L^2(-H, \eta(x))$ function space. Furthermore, the quantities $Z_{n,x}$ for each x in $a < x < b$ are defined by

$$[\![Z_{n,w}]\!] = \left[\frac{1}{\rho_j} \frac{\partial Z_n}{\partial w}\bigg|_{z=-h_j^+} - \frac{1}{\rho_{j+1}} \frac{\partial Z_n}{\partial w}\bigg|_{z=-h_j^-} \right], \quad j = 1, 2, \ldots, M-1. \tag{24}$$

Finally, from the last four terms in the left-hand side of the variational equation (15), defined on the vertical interfaces at $x = a$ and $x = b$, respectively, and considering the variations $\delta U_n(a)$, $\delta U_n(b)$, as well as $\delta B_n^{(1)}$ and $\delta A_n^{(3)}$, $n = -M+2, \ldots, 0, 1, \ldots$, we obtain the following end-conditions for the mode amplitudes U_n,

$$C_n^{(m)} dU_n/dx_1 + D_n^{(m)} U_n = F_n^{(m)}, \quad n = 0, 1, 2, \ldots, \; m = 1, 3, \tag{25a}$$

where $m = 1$ corresponds to the boundary condition at $x = a$ and $m = 3$ at $x = b$, respectively. The coefficients in the above equation supplemented the CMS (22) are defined as follows:

$$\begin{aligned} &C_n^{(m)} = 1, \qquad D_n^{(m)} = (-1)^{m+1}\, ik_n^{(m)}, \quad \text{for } n = 1, \ldots, N_p^{(m)}, \quad \text{and} \\ &C_n^{(m)} = 0, \qquad D_n^{(m)} = 1, \quad -M+2 \leq n \leq 0, \; m = 1, 2, \end{aligned} \tag{25b}$$

$$F_n^{(1)} = 2ik_n^{(1)} \exp\left(ik_n^{(1)} a\right) \delta_{\ell n} \quad \text{and} \quad F_n^{(2)} = 0, \quad n = 1, 2, \ldots, \tag{25c}$$

where $\delta_{\ell n}$ is Kronecker's delta and ℓ corresponds to the index of the incidence mode considered for exciting the waveguide. □

We note here that the applicability of the present method to similar 3D acoustic problems in cylindrically symmetric ocean environments, where the field is generated by a point 3D source, has been illustrated in Athanassoulis et al. [19]. In the latter work the resulting CMS has been numerically treated by using a second-order finite difference scheme based on a uniform grid on the horizontal plane. Also, detailed comparisons are presented against predictions by the finite element method and the coupled-modes based on the stairwise approximation, showing perfect agreement and validating the present approach. In the present work the CMS (22), (25) is discretized by applying the *hp*-FEM, which substantially improves

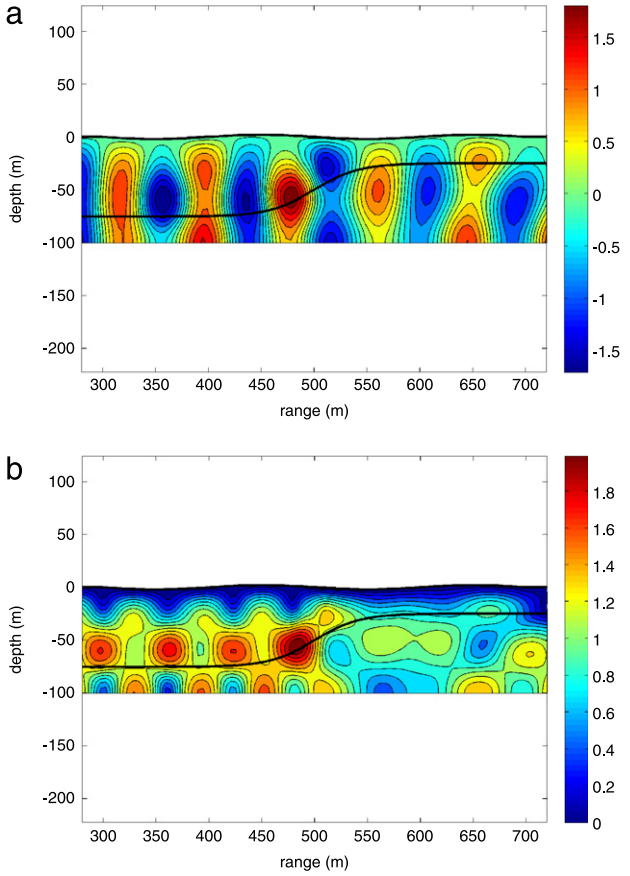

Fig. 2. Acoustic pressure in the waveguide as calculated by the present method. Excitation frequency 20 Hz and waveguide forcing by the first incident mode. Acoustic parameters: $\rho_1 = 1$ g/cm^3, $c_1 = 1500$ m/s, $\rho_2 = 1.5$ g/cm^3, $c_2 = 1700$ m/s. (a) Real part and (b) modulus of the wave field.

the numerical efficiency of the method and extends the domain of applicability to higher values of characteristic non-dimensional wavenumbers $\kappa \gg 1$. The theoretical background of the method and more details concerning the developed numerical scheme will be provided in Section 5.

In order to illustrate the numerical performance of the present model, as a first example, we consider here underwater acoustic propagation in simplified case consisting of two layers simulating a coastal acoustic environment, characterized by variable bathymetry. The geometry of the latter interface has the form of a smooth shoal, defined by

$$h_1(x) = 50 - 25 \tanh\left[3\pi\left(\left(\frac{x-300}{400}\right) - 0.5\right)\right], \quad a \le x \le b, \tag{26a}$$

where $a = 280$ m and $b = 720$ m; see Fig. 2. In this case, the max slope of the seabed reaches 60% in the middle of the variable bathymetry subdomain ($x = 500$ m) and the mean slope is 12.5%, respectively.

The upper layer (layer 1) corresponds to sea water of constant density and sound speed $\rho_1 = 1$ g/cm^3, $c_1 = 1500$ m/s. The lower layer (layer 2) under the seabed corresponds to sand–silt–clay sediment with properties $\rho_2 = 1.5$ g/cm^3, $c_2 = 1700$ m/s, terminated at the impermeable (rigid) bottom which is located at a depth $z = -100$ m. Furthermore, the upper surface $\eta(x)$ is modeled by a simple sinusoid, as follows

$$\eta(x) = -S_o \sin\left(k_s\,(x - 300)\right), \quad \text{in } 300 \text{ m} \le x \le 700 \text{ m}, \tag{26b}$$

and zero otherwise, where the amplitude of the free surface elevation is $S_o = 2$ m and the corresponding wavenumber $k_s = (4\pi/400)$ m^{-1}, modeling effect by quite long ripples of the sea surface (for example due to tidal waves) in the region.

In the examined two-layer case with constant parameters an analytical solution of VEP is available as described in Appendix A (see also [2]). This permits a very accurate calculation of all coefficients of the CMS Eq. (22), eliminating possible

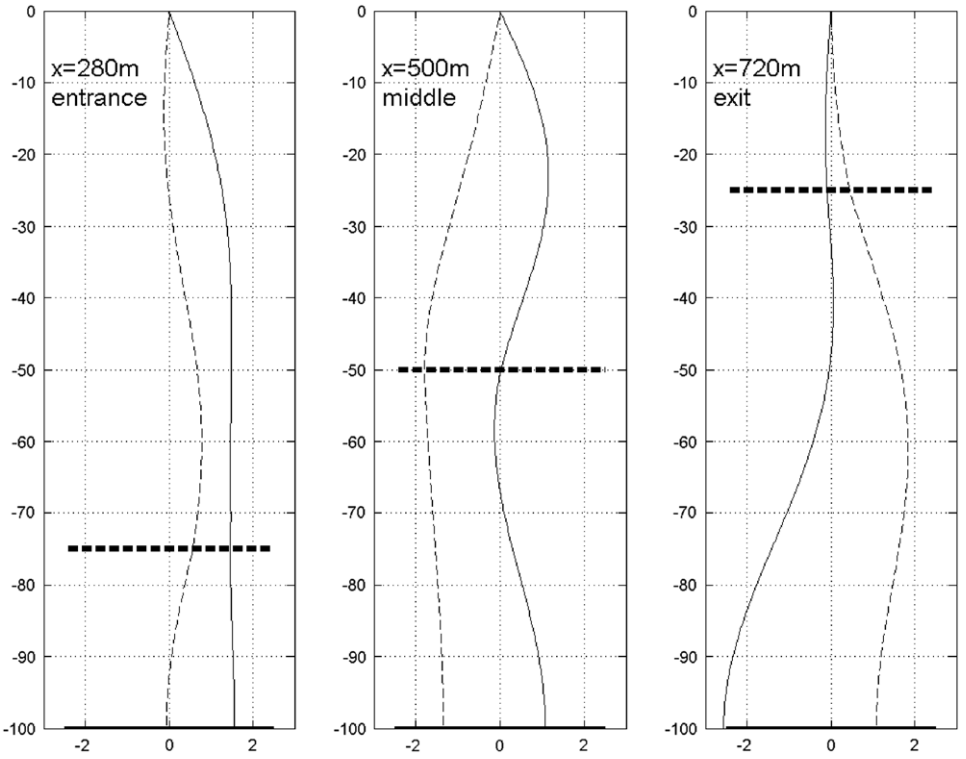

Fig. 3. Vertical distribution of the calculated wave field in the acoustic waveguide of Fig. 2 for the same excitation and frequency. Real part is shown by using solid lines and imaginary part by dashed lines.

errors entering through the numerical solution of the eigenvalue problem. The general treatment of the VEP by means of *hp*-FEM will be described in the next section, where the analytic solution in the two layer case will be used to show that it converges very rapidly, verifying the theoretical results concerning error estimation.

Numerical results concerning the real part of the calculated wave field, when the waveguide is excited at frequency $f = 20$ Hz and is forced by the first incident mode are shown in Fig. 2(a), as calculated by the *hp*-FEM using 4th degree polynomials ($p = 4$). The corresponding acoustic pressure modulus $|p(x, z)|$ is plotted in Fig. 2(b). In this case the characteristic nondimensional wavenumber is $\kappa \approx 37$. Also, the number of propagating modes is 3 both in the region of incidence and transmission. The local-mode series is truncated by keeping 15 totally modes, and the coupled-mode system is discretized using $N = 200$ elements based on uniform horizontal mesh, the same for all modes $U_n(x)$, $n = 0, 1, 2, \ldots, 14$, which were proved to be enough for numerical convergence. The corresponding vertical distributions of the wave field are presented in Fig. 3, at three horizontal positions, at the entrance, the middle, and exit of the waveguide. A higher-order solution of the above example obtained by using $p = 6$ and $N = 300$ will be used in Section 5 as a reference solution in order to demonstrate the convergence aspects of the present method, by illustrating the achieved rates of decay of the error with respect to mesh size (or number of elements) and polynomial degree.

Furthermore, in Fig. 4, the moduli of the modal-amplitude functions $|U_n(x)|$ are plotted vs. mode-number n, as calculated by the present CMS, with and without the additional sloping-interface mode, which in the examined two-layer case is only one $U_0(x)$. The horizontal axis in Fig. 4 is a multiple replica of the interval $[a,\ b]$, i.e. a sequence of repeated intervals $[a,\ b]$, each one associated with a mode, and named after the mode number. In the nth replica of interval $[a,\ b]$ the amplitude $|U_n(x)|$ of the nth mode is plotted vs. $x \in [a,\ b]$, as obtained by the present series with and without consideration of the additional sloping interface mode. We clearly observe the significance of the propagating modes ($n = 1, 2, 3$), in comparison to the evanescent modes ($n > 3$) and the additional mode ($n = 0$), which is of the same order of magnitude as the first evanescent modes. In the same figure the curve cn^{-4} is drawn (where c is a constant), using a thick black line. This curve bounds the maxima of the amplitudes of the modal functions as obtained by means of the enhanced representation Eq. (19), indicating that the rate of decay of the mode amplitudes is $O(n^{-4})$. The corresponding result based on the same system and the representation (16) without the additional interface mode ($n = 0$) is indicated by using red line, and we clearly observe that the rate of decay of the modal amplitudes is two-orders lower $O(n^{-2})$.

Another important conclusion that can be drawn from Fig. 4 deals with the improved efficiency of the present approach. Assuming that the error due to the truncation of the infinite modal series Eqs. (16) or (19) is of the same order as the last retained term in the truncated series, we obtain from Fig. 4 that for an error of the order of 0.2%, illustrated in the plot by using blue dashed lines, we need 9 totally terms ($n = 0, 1, 2, \ldots, 8$) with the enhanced representation, while without

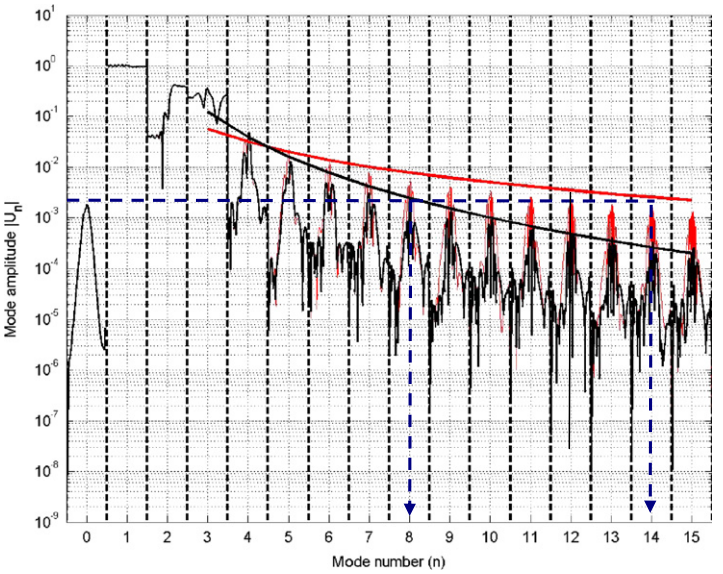

Fig. 4. Decay of modal amplitudes $|U_n|$ in the case of the waveguide of Fig. 2 excited by the first incident mode. The corresponding result without consideration of the additional sloping-interface mode is indicated by using the red line. (For interpretation of the references to colour in this figure legend, the reader is referred to the web version of this article.)

consideration of the additional mode the number of required terms is 14, and this difference is constantly increasing with frequency.

4. Finite element solution of the local vertical eigenvalue problem

In this section we will describe the application of the *hp*-Finite Element Method to the solution of the local VEP. Let $\Omega \doteq (-H, \eta(x))$ be the vertical interval at each horizontal position. All functions and parameters hereafter depend implicitly on x. Assuming that the density and acoustic wavenumber $\rho(z;x), k^2(z;x) \in L^\infty(\Omega)$, $a < x < b$, the following Sobolev spaces of real functions are introduced

$$W \doteq \left\{u : u \in H^1(\Omega) \text{ and } u(z=\eta(x)) = 0,\ x \in [a,b]\right\}.$$

The continuous vertical eigenvalue problem, at each horizontal position, is now stated in variational form as follows:

$$\text{Find } (\lambda, Z) \in \mathbb{R} \times W \text{ such that } \alpha(w,Z) = \lambda\beta(w,Z), \quad \forall w \in W, \tag{27}$$

where the involved bilinear forms are

$$\alpha(w,Z) = \int_{-H}^{\eta(x)} \rho^{-1} \frac{dw}{dz}\frac{dZ}{dz}dz - \int_{-H}^{\eta(x)} \rho^{-1} w\, k^2 Z\, dz, \quad \text{and} \tag{28a}$$

$$\beta(w,Z) = \int_{-H}^{\eta(x)} \rho^{-1} w Z dz. \tag{28b}$$

Assume also a partition of $\bar{\Omega}$ of the form $-H = z_1 < z_2 < \cdots < z_{N+1} = \eta(x)$, with $N \in \mathbb{N}$ and $N > M$ (M being the number of layers in the waveguide). The partition is such that for every position along x-axis, the interface positions $z = -h_j(x)$, $j = 1, 2, \ldots, M-1$, coincide with $M-1$ nodes. We introduce the sequence of finite element sub-spaces $W^h \subset W$

$$W^h \doteq \left\{u^h \in H^1(\Omega) : u^h\big|_{[z_i, z_{i+1}]} \equiv P_\ell(z) \text{ and } u^h(z=\eta(x)) = 0, i = 1, 2, \ldots, N,\ \ell \in \mathrm{N},\ x \in [a,b]\right\}$$

where $P_\ell(z)$ is a polynomial of degree ℓ. The discrete variational formulation of the VEP takes the following form:

$$\text{Find } (\lambda^h, Z^h) \in \mathbb{R} \times W^h \text{ such that } \alpha(w^h, Z^h) = \lambda^h \beta(w^h, Z^h), \quad \forall w^h \in W^h. \tag{29}$$

Remark 1. Adding the term $\Lambda \int_{-H}^{\eta(x)} \rho^{-1} w Z dz$, where $\Lambda \in \mathbb{R}$, in Eq. (28a), simply shifts the eigenvalues by Λ and has no effect on the eigenvectors. The same is also valid for the discrete eigenvalues and eigenfunctions of the discrete formulation (29). Let $\tilde{\lambda} \in \mathbb{R}, \tilde{Z} \in W$, denote the new eigenpairs. The modified version of the eigenvalue problem is:

$$\text{Find } (\tilde{\lambda}, \tilde{Z}) \in \mathbb{R} \times W \text{ such that } \alpha(w, \tilde{Z}) = \left(\tilde{\lambda} - \Lambda\right)\beta(w, \tilde{Z}), \quad \forall w \in W. \tag{30}$$

Comparing the above versions it is easy to confirm that $\tilde{Z}(x) = Z(x)$ and $\tilde{\lambda} = \Lambda + \lambda$. The steps to prove the same result for the discrete formulation are identical. Thus, we arrive at the following

Theorem 2. *Let $d_k(x) = ess\,sup_{z\in\Omega} k^2(z;x)$, $d_\rho = \max_j\{\rho_j\}$ and assume that $\Lambda \geq d_k + \varepsilon$ for some $\varepsilon \geq \kappa^2$, where $\kappa = 1\,\mathrm{m}^{-1}$. Then, the bilinear form, $\gamma(w,Z) \doteq \alpha(w,Z) + \Lambda\beta(w,Z)$, becomes W-elliptic with ellipticity constant $\mu = d_\rho^{-1}$. That is, $\forall Z \in W$ it is $\gamma(Z,Z) \geq \mu \|Z\|^2_{1,\Omega}$.*

Proof. It is

$$\gamma(Z,Z) = \int_{-H}^{\eta} \rho^{-1}\frac{dZ}{dz}\frac{dZ}{dz}dz + \int_{-H}^{\eta}\left(\Lambda - k^2\right)\rho^{-1}Z^2 dz \geq \frac{1}{d_\rho}\int_{-H}^{\eta}\left(\frac{dZ}{dz}\right)^2 dz + \frac{\Lambda - d_k}{d_\rho}\int_{-H}^{\eta} Z^2 dz$$

and thus,

$$\gamma(Z,Z) \geq \frac{\kappa^2}{d_\rho}|Z|^2_{1,\Omega} + \frac{\Lambda - d_k}{d_\rho}\|Z\|^2_{0,\Omega} \geq \frac{\kappa^2}{d_\rho}|Z|^2_{1,\Omega} + \frac{\varepsilon}{d_\rho}\|Z\|^2_{0,\Omega} \geq \mu\|Z\|^2_{1,\Omega}, \quad \text{where } \mu = min\left\{\kappa^2, \varepsilon\right\}/d_\rho.$$

The optimal value is derived for $\varepsilon = \kappa^2$, which provides the desired result. □

Based on the above, we may now use the properties of the modified problem (30) in order to derive a priori bounds for the eigenvalues of our initial eigenvalue problem. To this respect, from $\tilde{\lambda} = \frac{\gamma(\tilde{Z},\tilde{Z})}{\beta(\tilde{Z},\tilde{Z})} \geq \frac{c_\rho \mu \|\tilde{Z}\|^2_{1,\Omega}}{\|\tilde{Z}\|^2_{1,\Omega}}$ we obtain $\tilde{\lambda} \geq \frac{c_\rho}{d_\rho}$, where $c_\rho = \min_j\{\rho_j\}$. Thus, we have for the eigenvalues λ of problem (27), the following estimation

$$\lambda \geq \frac{c_\rho}{d_\rho} - d_k - \kappa^2. \tag{31}$$

4.1. Numerical solution of VEP by hp-FEM

The discrete solution has the form

$$Z^h(z) = \sum_{j=1}^{N} q_j N_j(z), \tag{32}$$

where $N_j \in W^h$. Introducing the above expansion in Eq. (29), the discrete variational formulation finally becomes an eigenvalue matrix equation of the form:

$$\mathbf{A}_{VEP}\,\mathbf{q} = \lambda\,\mathbf{B}_{VEP}\,\mathbf{q}, \tag{33}$$

where the elements of the $N \times N$ matrices $\mathbf{A}_{VEP}$ and $\mathbf{B}_{VEP}$ are $\alpha_{ij} = \alpha(N_i, N_j)$ and $\beta_{ij} = \beta(N_i, N_j)$, $i,j = 1,2,\ldots,N$, respectively, and $\mathbf{q} = q_j$. From the above results, the optimality of the Galerkin method for standard elliptic eigenvalue problems is deduced [35] and the following error estimates are valid

$$\lambda_n \leq \lambda_n^h \leq \lambda_n + c\lambda_n^{(\ell+1)}h^{2\ell}, \tag{34a}$$

$$\left\|Z_n^h - Z_n\right\|_{H^1(\Omega)} \leq c\lambda_n^{(\ell+1)/2}h^\ell \tag{34b}$$

where c is a positive constant independent of h and λ_n.

Further, the following L^2-estimate for the eigenfunction convergence is valid:

$$\left\|Z_n^h - Z_n\right\|_{L^2(\Omega)} \leq c\lambda_n^{(\ell+1)/2}h^{\ell+1}. \tag{35}$$

It is evident from the above results that the quality of the approximation deteriorates as the magnitude of the eigenvalue approximated increases. This fact will be also confirmed by the results of the convergence diagrams presented and discussed in the sequel.

As an example, we consider the case of an acoustic environment of total thickness (depth) $H = 100$ m, and flat free surface $\eta = 0$, consisting of two layers of equal thickness, and thus the position of the internal interface is at a depth $h_1 = 50$ m. The acoustic parameters and the frequency are assumed the same as before ($f = 20$ Hz, $\rho_1 = 1$ g/cm^3, $c_1 = 1500$ m/s, $\rho_2 = 1.5$ g/cm^3, $c_2 = 1700$ m/s). In this case an exact analytical solution of the VEP is available (see also Boyles [2]) and details are provided in Appendix A.

Fig. 5 shows the first 30 eigenvalues as computed by the present FEM, using $p = 1$ and $p = 2$, using $N = 40, 80, 160$ elements, compared against the exact solution. As expected, the error of the numerical solution is found to increase with increasing eigenvalue numbers. Fig. 6 is a log–log plot depicting the convergence of the finite element solution for the 5th, 10th and 15th eigenvalue, for $p = 1, 2$ and 3, with increasing number of elements. The observed order of the rate of

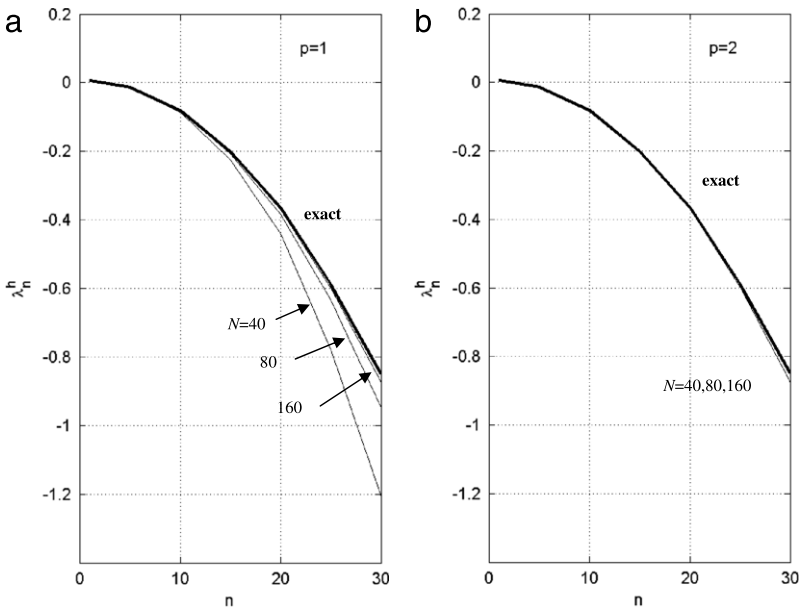

Fig. 5. Comparison of computed eigenvalues against the exact solution (shown by using the thick line) for different numbers of elements N, and using (a) $p = 1$ and (b) $p = 2$.

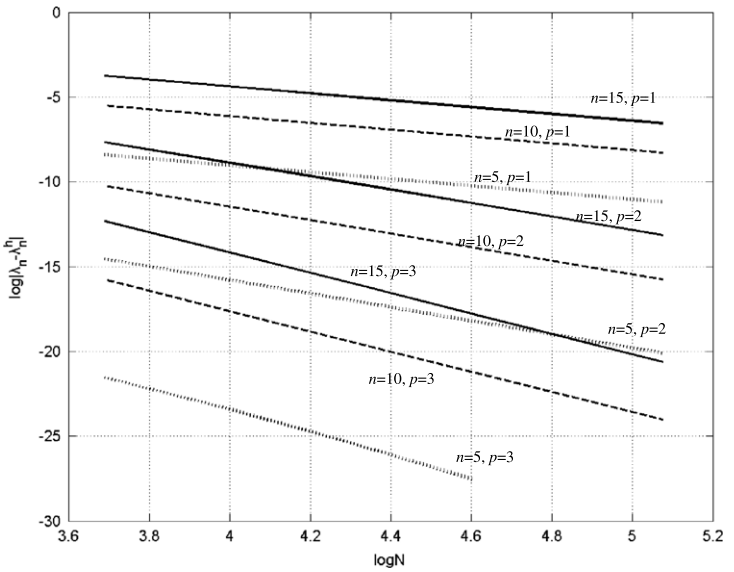

Fig. 6. Convergence plot concerning the computed 5th (dotted lines), 10th (dashed lines) and 15th (solid lines) eigenvalues against the number of elements N, by using $p = 1, 2, 3$.

convergence is 2, 4 and 6, respectively, and is found to be in full agreement with Eq. (34a). Also from this figure it becomes clear the substantial improvement of the efficiency of approximation by increasing the degree of the polynomials.

Moreover, the first 4 eigenfunctions, as computed using the present FEM with $N = 160$ and $p = 3$, are plotted in Fig. 7. In this case the present numerical results agree perfectly with the analytical solution and the differences cannot be distinguished at the scale of the figure. A log–log plot is shown in Fig. 8 concerning the error in comparison to the exact solution

$$\left\| Z_n^h - Z_n \right\|_{H^1(-H,\eta)} = \left[\int_{-H}^{\eta} \left(Z_n^h - Z_n \right)^2 dz + \int_{-H}^{\eta} \left(dZ_n^h/dz - dZ_n/dz \right)^2 dz \right]^{1/2}, \tag{36}$$

demonstrating the convergence of the 5th, 10th and 15th eigenfunction in the $H^1(-H, \eta)$ norm. The computations are again based on $N = 40, 80, 160$ elements. As expected, the observed rate of convergence for $p = 1, 2, 3$ is found to be 1, 2 and 3,

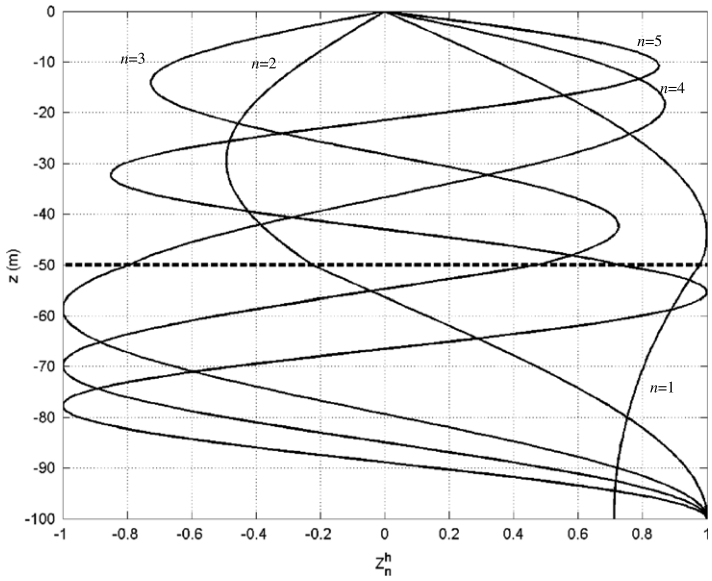

Fig. 7. Vertical plot of the first 5 eigenfunctions, as calculated by the present FEM ($p = 3$) using $N = 160$ elements. The position of the interface is indicated by using a horizontal dashed line.

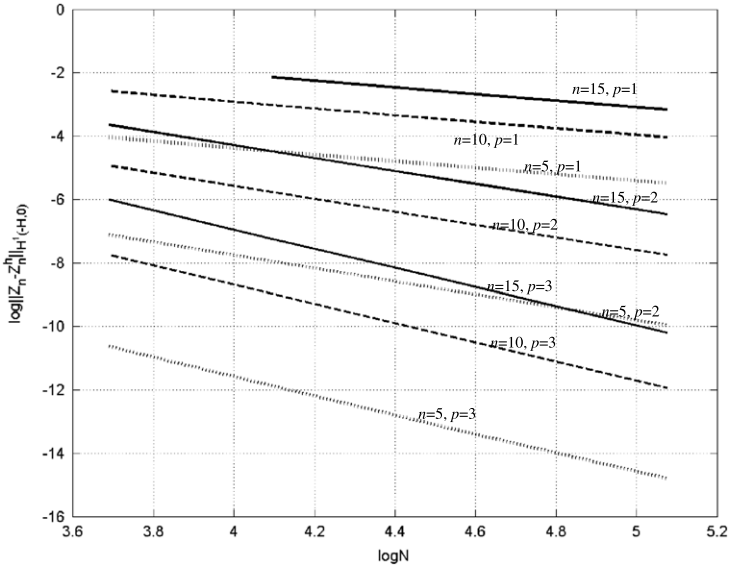

Fig. 8. Convergence plot concerning the 5th (dotted lines), 10th (dashed lines) and 15th (solid lines) eigenfunctions $Z_n(z)$ calculated by the present FEM in the $H^1(-H, \eta)$ norm, against the number of elements N, by using $p = 1, 2, 3$.

respectively, which is in full conformity with the prediction stated in Eq. (34b). Enhanced rates are obtained by raising the degree of the piecewise polynomials. We conclude this subsection by remarking that the present VEP-FEM solver provides highly accurate numerical solutions in complex multilayered waveguides with small computational cost.

On the basis of the above numerical solution, in conjunction with the expressions of the additional sloping-interface vertical modes, given by Eq. (20b), the CMS matrix coefficients a_{mn}, b_{mn}, and c_{mn}, are very efficiently calculated all over the horizontal plane by vertical integration using Gaussian quadrature.

5. Numerical solution of the CMS using adaptive *hp*-FEM

For the approximate solution of present CMS Eq. (22), in conjunction with the corresponding boundary conditions Eqs. (25), the local-mode series Eq. (19) is truncated keeping except of the propagating, a finite number of evanescent modes and the additional sloping-interface modes. Let n_1 be the total number of retained propagating and evanescent modes (with

index $n > 0$) and $n_0 = M - 1$ the number of sloping-interface terms (with index $n \leq 0$). The total number of retained terms is then $N_m = n_0 + n_1$, which equals to the dimension of the truncated system.

Let $x \in (a, b)$ and $\mathbb{M}_{n_1\times n_1}$, $\mathbb{M}_{N_m\times N_m}$ denote the set of $n_1 \times n_1$ and $N_m \times N_m$ real matrices respectively. Assuming that matrix $[a_{mn}]$ is invertible, the truncated coupled mode system (22) takes the form:

$$-\boldsymbol{v}'' + \boldsymbol{B}\boldsymbol{v}' + \boldsymbol{C}\,\boldsymbol{v} = \boldsymbol{0}, \quad x \in (a, b)\,, \tag{37}$$

where a prime is used to denote x-differentiation, and $\boldsymbol{B} = -[a_{mn}]^{-1}[b_{mn}]$, $\boldsymbol{C} = -[a_{mn}]^{-1}[c_{mn}]$. In the above equation $\boldsymbol{v}$ is the column vector of unknown complex modal amplitudes $\boldsymbol{v} \doteq conj\left([\boldsymbol{v}_0\boldsymbol{v}_1]^T\right)$, where $\boldsymbol{v}_0 \doteq \begin{pmatrix} U_{-M+2}(x) & U_{-M+1}(x) & \dots & U_0(x)\end{pmatrix}$ and $\boldsymbol{v}_1 \doteq \begin{pmatrix} U_1(x) & U_2(x) & \dots & U_{n_1}(x)\end{pmatrix}$. The system is supplemented by the following boundary conditions

$$\boldsymbol{v}_0 = \boldsymbol{0}, \quad \text{and} \quad \boldsymbol{v}_1' + \boldsymbol{S}_1\boldsymbol{v}_1 = \boldsymbol{T}_1, \quad \text{at } x = a, \tag{38a}$$

$$\boldsymbol{v}_0 = \boldsymbol{0}, \quad \text{and} \quad \boldsymbol{v}_1' + \boldsymbol{S}_2\boldsymbol{v}_1 = \boldsymbol{T}_2, \quad \text{at } x = b, \tag{38b}$$

where $\boldsymbol{S}_1, \boldsymbol{S}_2 \in \mathbb{M}_{n_1\times n_1}$ are diagonal matrices and $\boldsymbol{T}_1, \boldsymbol{T}_2 \in \mathbb{C}^{n_1}$; see Eqs. (25).

In order to proceed with the analysis of the variational form of the above boundary value problem Eqs. (37), (38) it is convenient to work with homogeneous Robin-type boundary conditions. We have the following result.

Theorem 3. *Set* $\boldsymbol{D} = \boldsymbol{I} - \boldsymbol{S}_1\left((b-a)\boldsymbol{I} + \boldsymbol{S}_2^{-1}\right)$. *Let* $\boldsymbol{v} = \boldsymbol{u} + \boldsymbol{F}_1 x + \boldsymbol{F}_2$ *be the solution of boundary value problem* (37), (38). *Then* $\boldsymbol{u} = conj\begin{pmatrix}\boldsymbol{u}_0 & \boldsymbol{u}_1\end{pmatrix}^T$ *is obtained as the solution of boundary value problem*

$$-\boldsymbol{u}'' + \boldsymbol{B}\boldsymbol{u}' + \boldsymbol{C}\boldsymbol{u} = -\left(\boldsymbol{C}\boldsymbol{F}_1 x + \boldsymbol{B}\boldsymbol{F}_1 + \boldsymbol{C}\boldsymbol{F}_2\right) \equiv \boldsymbol{F}, \quad x \in (a, b)\,, \tag{39}$$

$$\boldsymbol{u}_0 = \boldsymbol{0}, \qquad \boldsymbol{u}_1' + \boldsymbol{S}_1\boldsymbol{u}_1 = \boldsymbol{0} \quad \text{at } x = a, \tag{40a}$$

$$\boldsymbol{u}_0 = \boldsymbol{0}, \qquad \boldsymbol{u}_1' + \boldsymbol{S}_2\boldsymbol{u}_1 = \boldsymbol{0}, \quad \text{at } x = b, \tag{40b}$$

where the forcing $\boldsymbol{F}$ *of the differential system is given by*

$$\boldsymbol{F}_1 = \begin{bmatrix}\boldsymbol{0}_{n_0\times 1} \\ \boldsymbol{D}^{-1}\left(\boldsymbol{T}_1 - \boldsymbol{S}_1\boldsymbol{S}_2^{-1}\boldsymbol{T}_2\right)\end{bmatrix} \quad \text{and} \quad \boldsymbol{F}_2 = \begin{bmatrix}\boldsymbol{0}_{n_0\times 1} \\ \boldsymbol{S}_2^{-1}\left(\boldsymbol{T}_2 - (\boldsymbol{I} + b\boldsymbol{S}_2)\,\boldsymbol{D}^{-1}\left(\boldsymbol{T}_1 - \boldsymbol{S}_1\boldsymbol{S}_2^{-1}\boldsymbol{T}_2\right)\right)\end{bmatrix}. \tag{41}$$

Proof. From Eqs. (38), we have

$$\boldsymbol{u}_1' + \boldsymbol{S}_1\boldsymbol{u}_1 + (\boldsymbol{I} + a\boldsymbol{S}_1)\,\boldsymbol{F}_1 + \boldsymbol{S}_1\boldsymbol{F}_2 = \mathbf{T}_1, \quad \text{at } x = a, \tag{42a}$$

$$\boldsymbol{u}_1' + \boldsymbol{S}_2\boldsymbol{u}_1 + (\boldsymbol{I} + b\boldsymbol{S}_2)\,\boldsymbol{F}_1 + \boldsymbol{S}_2\boldsymbol{F}_2 = \mathbf{T}_2, \quad \text{at } x = b. \tag{42b}$$

For the above conditions to be homogeneous, it must be

$$\begin{bmatrix}\boldsymbol{I} + a\boldsymbol{S}_1 & \boldsymbol{S}_1 \\ \boldsymbol{I} + b\boldsymbol{S}_2 & \boldsymbol{S}_2\end{bmatrix}\begin{bmatrix}\boldsymbol{F}_1 \\ \boldsymbol{F}_2\end{bmatrix} = \begin{bmatrix}\boldsymbol{T}_1 \\ \boldsymbol{T}_2\end{bmatrix}. \tag{43}$$

The matrix $\boldsymbol{D} = \boldsymbol{I} - \boldsymbol{S}_1\left((b-a)\boldsymbol{I} + \boldsymbol{S}_2^{-1}\right)$ is the Schur complement of $\boldsymbol{S}_2$ with respect to the partitioned matrix in (43). Since both $\boldsymbol{S}_2$ and $\boldsymbol{D}$ are invertible, the partitioned matrix is invertible and the solution is given by Eq. (41). □

5.1. Notation and preliminaries

We consider the function spaces

$$H = \left[L^2(a, b)\right]^{N_m} \doteq L^2(a, b) \times L^2(a, b) \times \underbrace{\dots\dots\dots}_{N_m \text{ times}} \times L^2(a, b) \quad \text{and} \quad V = \left[H_0^1(a, b)\right]^{n_0} \times \left[H^1(a, b)\right]^{n_1}, \tag{44}$$

where $H^1(a, b)$, $H_0^1(a, b)$ denotes the Sobolev spaces $W^{1,2}(a, b)$ and $W_0^{1,2}(a, b) \doteq \{u : u \in W_0^{1,2}(a, b) \text{ and } u(a) = u(b) = 0\}$ in the horizontal interval $a < x < b$, respectively; see, e.g., Ref. [36]. Note that all function spaces are defined over $\mathbb{C}$. The standard inner products in H, V are denoted as $(\cdot,\cdot)_H$, $(\cdot,\cdot)_V$ respectively. Moreover, for $\boldsymbol{u} \doteq conj\begin{pmatrix}u_1 & u_2 & \dots & u_{n_2}\end{pmatrix}^T \in V$, we denote $\|\boldsymbol{u}\|_V = \left(\sum_{k=1}^{N_m}\|u_k\|^2_{H^1(a,b)}\right)^{1/2}$, the standard Hilbert space norm and $|\boldsymbol{u}|_V$ the corresponding semi-norm. Further it is $\|\boldsymbol{u}\|_H = \left(\sum_{k=1}^{N_m}\|u_k\|^2_{L^2(a,b)}\right)^{1/2}$. From the above definitions we have that V is a dense subspace of H and thus, there exists $\mathrm{K}_1 \in (0, \infty)$ such that $\|\boldsymbol{u}\|_H \leq \mathrm{K}_1\|\boldsymbol{u}\|_V, \forall \boldsymbol{u} \in V$. In the following, the value $\mathrm{K}_1 = 1$ will be adopted.

Next, a sesquilinear functional $p(\boldsymbol{u}, \boldsymbol{w})$, $\boldsymbol{u}, \boldsymbol{w} \in V$ is of sectorial form (see Ref. [37]), if there exist $c \in \mathbb{R}$, $\mathrm{K}_2 \in (0, \infty)$, $\mathrm{K}_3 \in (0, \infty)$ such that

$$|p(\boldsymbol{u}, \boldsymbol{w})| \leq \mathrm{K}_2 \|\boldsymbol{u}\|_V \|\boldsymbol{w}\|_V, \quad \forall \boldsymbol{u}, \boldsymbol{w} \in V, \quad \text{and} \tag{45}$$

$$\mathrm{Re}[p(\boldsymbol{u}, \boldsymbol{u})] \geq \mathrm{K}_3 \|\boldsymbol{u}\|_V^2 + c \|\boldsymbol{u}\|_H^2, \quad \forall \boldsymbol{u} \in V, \tag{46}$$

which is a Gårding type inequality for $p(\boldsymbol{u}, \boldsymbol{w})$.

Moreover, for any matrix $\boldsymbol{G} \in \mathbb{M}_{n_2 \times n_2}$ we denote $\boldsymbol{G}_S$ and $\boldsymbol{G}_A$ the symmetric and skew-symmetric part of $\boldsymbol{G}$, respectively. Consequently, $\mathrm{Re}[\boldsymbol{y}^* \boldsymbol{G}_A \boldsymbol{y}] = 0$, $\forall \boldsymbol{y} \in \mathbb{C}^{n_2}$. In the sequel use will be made of following

Lemma 1. *Let $\mathbf{G} \in \mathbb{M}_{n_2 \times n_2}$, $\mathbf{y} \in V$ and the elements of matrix $\mathbf{G}$ satisfy $g_{ij}(x) \in W^{1,\infty}(a, b)$. It holds*

$$\int_a^b 2Re[\mathbf{u}^* \mathbf{G}_S \mathbf{u}'] \, dx = \int_a^b Re[(\mathbf{u}^* \mathbf{G} \mathbf{u})'] \, dx - \int_a^b Re[\mathbf{u}^* \mathbf{G}_S' \mathbf{u}] \, dx. \tag{47}$$

The result is obtained by simple application of integration by parts, and by using the identities $Re[\mathbf{y}^{*\prime} \mathbf{G}_A \mathbf{y}] = -Re[\mathbf{y}^* \mathbf{G}_A \mathbf{y}']$ and $Re[\mathbf{y}^{*\prime} \mathbf{G}_S \mathbf{y}] = \mathrm{Re}[\mathbf{y}^* \mathbf{G}_S \mathbf{y}']$.

The main tool for obtaining finite element approximations of the variational form of boundary value problem Eqs. (39), (40) is the following result for sectorial sesquilinear forms (see also Ref. [37]):

Lemma 2. *Let V^h be a closed subspace of V, $f \in H$, $\vartheta \in [0, \mathrm{K}_3)$, $\varphi \in \mathbb{C}$, $Re[\varphi] \leq c + \vartheta \mathrm{K}_1^{-2}$. Also, let $u \in V$ be the unique solution of the following variational problem*

$$p(u, w) = (\varphi u + f, w)_H, \quad \forall w \in V. \tag{48}$$

Then, there exists unique $u_h \in V^h$ such that $p(u_h, w_h) = (\varphi u_h + f, w_h)_H$, $\forall w_h \in V^h$. Moreover it is $\|u_h\|_H \leq \left(\mathrm{K}_3 \mathrm{K}_1^{-2} + c - Re[\varphi]\right)^{-1} \|f\|_H$, $\|u_h\|_V^2 \leq (\mathrm{K}_3 - \vartheta)^{-1} \|u_h\|_H \|f\|_H$ and

$$\|u_h - u\|_V \leq \frac{\mathrm{K}_2 + |\varphi| \, \mathrm{K}_1^2}{\mathrm{K}_3 - \vartheta} \inf_{v \in V^h} \|v - u\|_V. \tag{49}$$

Closing the presentation of preliminary results, we recall the arithmetic–geometric mean inequality for any real numbers r_1, r_2 and $\sigma > 0$

$$r_1 r_2 \leq \frac{\sigma}{2} r_1^2 + \frac{1}{2\sigma} r_2^2. \tag{50}$$

5.2. Variational formulation and finite element approximation of the CMS

The variational formulation of the boundary value problem associated with the present CMS is written as follows.
Find $\boldsymbol{u} \in V$ such that

$$\int_a^b \boldsymbol{w}^{*\prime} \boldsymbol{u}' dx + \int_a^b \boldsymbol{w}^* \boldsymbol{B} \boldsymbol{u}' dx + \int_a^b \boldsymbol{w}^* \boldsymbol{C} \boldsymbol{u} dx + \boldsymbol{w}^*(b) \boldsymbol{S}_2 \boldsymbol{u}(b) - \boldsymbol{w}^*(a) \boldsymbol{S}_1 \boldsymbol{u}(a) = \int_a^b \boldsymbol{w}^* \boldsymbol{F} dx, \quad \forall \boldsymbol{w} \in V \tag{51}$$

where $\boldsymbol{w}^* = conj\left(\boldsymbol{w}^T\right)$. From Eq. (51), we define, the following sesquilinear form $p(\cdot, \cdot) : V \times V \to \mathbb{C}$

$$p(\boldsymbol{u}, \boldsymbol{w}) \equiv \int_a^b \boldsymbol{w}^{*\prime} \boldsymbol{u}' dx + \int_a^b \boldsymbol{w}^* \boldsymbol{B} \boldsymbol{u}' dx + \int_a^b \boldsymbol{w}^* \boldsymbol{C} \boldsymbol{u} dx + \boldsymbol{w}^*(b) \boldsymbol{S}_2 \boldsymbol{u}(b) - \boldsymbol{w}^*(a) \boldsymbol{S}_1 \boldsymbol{u}(a), \tag{52}$$

and the variational formulation (51) is written (see also (39)) as follows:

$$\text{Find } \boldsymbol{u} \in V \text{ such that } p(\boldsymbol{u}, \boldsymbol{w}) = f(\boldsymbol{w}) \equiv \int_a^b \boldsymbol{w}^* \boldsymbol{F} dx, \quad \forall \boldsymbol{w} \in V. \tag{53}$$

In the sequel, existence and uniqueness of weak solutions of the above variational problem will be studied, permitting implementation of corresponding finite element approximation. To this direction, we introduce the following assumptions:

(A1) For the elements of matrices $\boldsymbol{B}, \boldsymbol{C}$, it is $b_{ij}(x) \in W^{1,\infty}(a, b)$, $c_{ij}(x) \in L^\infty(a, b)$, $i, j = 1, 2, \ldots, N_m$.
(A2) There exists a function $\boldsymbol{S}$: $[a, b] \to \mathbb{M}_{n_1 \times n_1}$, such that $\boldsymbol{S}(a) = \boldsymbol{S}_1$, $\boldsymbol{S}(b) = \boldsymbol{S}_2$ and $s_{ij}(x) \in W^{1,\infty}(a, b)$, $i, j = 1, 2, \ldots, n_1$.

In the above assumptions, all function spaces are defined over $\mathbb{C}$. It is straightforward to prove continuity of the above functional Eq. (52). We then obtain the result stated in the following

Theorem 4. *Let $p(\cdot,\cdot): V\times V\to\mathbb{C}$ be defined through (52) and assumptions* (A1), (A2) *hold. Then $|p(\boldsymbol{u},\boldsymbol{w})|\le \mathrm{K}_2\|\boldsymbol{u}\|_V\|\boldsymbol{w}\|_V$, $\forall \boldsymbol{u},\boldsymbol{w}\in V$, with $\mathrm{K}_2=1+\|\!|\boldsymbol{B}|\!\|_\infty+\|\!|\boldsymbol{C}|\!\|_\infty+2\|\!|\boldsymbol{S}|\!\|_\infty+\|\!|\boldsymbol{S}'|\!\|_\infty$, where $\|\!|\boldsymbol{Q}|\!\|_\infty \doteq \underset{x\in[a,b]}{ess\,sup}\{\|\boldsymbol{Q}\|_2\}$, for a matrix $\boldsymbol{Q}$.*

The detailed proof is provided in Appendix B. □

Furthermore, from the boundary conditions of the CMS, Eqs. (25), and the distribution of the vertical eigenvalues at the ends $x=a$ and $x=b$ of the inhomogeneous domain, we see that

$$b_{ij}(a)=b_{ij}(b)=0,\quad i,j=1,2,\ldots,N_m,\quad \text{and} \tag{54a}$$

$$\mathrm{Re}[\boldsymbol{v}^*(b)\boldsymbol{S}_2\boldsymbol{v}(b)-\boldsymbol{v}^*(a)\boldsymbol{S}_1\boldsymbol{v}(a)]=\sum_{(ev)}k_n^{(3)}\,|U_n(b)|^2+k_n^{(1)}\,|U_n(a)|^2\ge 0, \tag{54b}$$

with the summation considered over the evanescent modes. Taking this into account, we state the following result in order to establish a Gårding-type inequality for $p(\boldsymbol{u},\boldsymbol{w})$:

Theorem 5. *Let $p(\cdot,\cdot): V\times V\to\mathbb{C}$ be defined through Eq. (52), and* (A1), (A2) *hold. Select $2\sigma>\|\!|\boldsymbol{B}_A|\!\|_\infty$, $\sigma\in\mathbb{R}^+$ and assume there exists $\xi\in\mathbb{R}^+$, such that $\forall\boldsymbol{u}\in V$ it holds*

$$Re\left[\boldsymbol{u}^*\left(\boldsymbol{C}-\frac{1}{2}\boldsymbol{B}'\right)_S\boldsymbol{u}\right]\ge\xi\boldsymbol{u}^*\boldsymbol{u}. \tag{55}$$

Then, $Re[p(\boldsymbol{u},\boldsymbol{u})]\ge \mathrm{K}_3\,\|\boldsymbol{u}\|_V^2+c\,\|\boldsymbol{u}\|_H^2$, with $\mathrm{K}_3=1-\frac{1}{2\sigma}\|\!|\boldsymbol{B}_A|\!\|_\infty$ and $c=\xi-1+\frac{1-\sigma^2}{2\sigma}\|\!|\boldsymbol{B}_A|\!\|_\infty$.

Proof. From Eq. (52), the definitions of the norm and seminorm in V and assumption (A2),

$$\begin{aligned}p(\boldsymbol{u},\boldsymbol{u}) &= \int_a^b\boldsymbol{u}^{*\prime}\boldsymbol{u}'dx+\int_a^b\boldsymbol{u}^*\boldsymbol{B}\boldsymbol{u}'dx+\int_a^b\boldsymbol{u}^*\boldsymbol{C}\boldsymbol{u}dx+\boldsymbol{u}^*(b)\boldsymbol{S}_2\boldsymbol{u}(b)-\boldsymbol{u}^*(a)\boldsymbol{S}_1\boldsymbol{u}(a)\\ &= |\boldsymbol{u}|_V^2+\int_a^b\boldsymbol{u}^*\boldsymbol{B}\boldsymbol{u}'dx+\int_a^b\boldsymbol{u}^*\boldsymbol{C}\boldsymbol{u}dx+\boldsymbol{u}^*(b)\boldsymbol{S}_2\boldsymbol{u}(b)-\boldsymbol{u}^*(a)\boldsymbol{S}_1\boldsymbol{u}(a),\quad\text{and}\end{aligned}$$

$$\mathrm{Re}[p(\boldsymbol{u},\boldsymbol{u})]=|\boldsymbol{u}|_V^2+\int_a^b\mathrm{Re}[\boldsymbol{u}^*\boldsymbol{B}\boldsymbol{u}']dx+\int_a^b\mathrm{Re}[\boldsymbol{u}^*\boldsymbol{C}\boldsymbol{u}]dx+\mathrm{Re}[\boldsymbol{u}^*(b)\boldsymbol{S}_2\boldsymbol{u}(b)-\boldsymbol{u}^*(a)\boldsymbol{S}_1\boldsymbol{u}(a)]. \tag{56}$$

Then, from Eq. (56), Lemma 1, and Eqs. (54), we obtain

$$\mathrm{Re}[p(\boldsymbol{u},\boldsymbol{u})]\ge|\boldsymbol{u}|_V^2+\int_a^b\mathrm{Re}[\boldsymbol{u}^*\boldsymbol{B}_A\boldsymbol{u}']dx+\int_a^b\mathrm{Re}\left[\boldsymbol{u}^*\left(\boldsymbol{C}-\frac{1}{2}\boldsymbol{B}'\right)_S\boldsymbol{u}\right]dx. \tag{57}$$

For the first integral in the right-hand side of the above relation we have

$$\left|\int_a^b\mathrm{Re}[\boldsymbol{u}^*\boldsymbol{B}_A\boldsymbol{u}']dx\right|\le\int_a^b\left|\mathrm{Re}[\boldsymbol{u}^*\boldsymbol{B}_A\boldsymbol{u}']\right|dx\le\int_a^b\mathrm{Re}[|\boldsymbol{u}^*\boldsymbol{B}_A\boldsymbol{u}'|]dx=\int_a^b\left|\boldsymbol{u}^*\boldsymbol{B}_A\boldsymbol{u}'\right|dx. \tag{58}$$

Furthermore, using Cauchy–Schwarz inequality we obtain

$$\int_a^b\left|\boldsymbol{u}^*\boldsymbol{B}_A\boldsymbol{u}'\right|dx\le\left(\int_a^b\left|\boldsymbol{u}^*\right|^2dx\right)^{1/2}\left(\int_a^b\left|\boldsymbol{B}_A\boldsymbol{u}'\right|^2dx\right)^{1/2}\le\left(\int_a^b\left|\boldsymbol{u}^*\right|^2dx\right)^{1/2}\left(\int_a^b\|\boldsymbol{B}_A\|^2\left|\boldsymbol{u}'\right|^2dx\right)^{1/2}, \tag{59}$$

and finally,

$$\left|\int_a^b\mathrm{Re}[\boldsymbol{u}^*\boldsymbol{B}_A\boldsymbol{u}']dx\right|\le\|\!|\boldsymbol{B}_A|\!\|_\infty\,\|\boldsymbol{u}\|_H\,|\boldsymbol{u}|_V\,. \tag{60}$$

In view of the above result, Eq. (57) becomes

$$\mathrm{Re}[p(\boldsymbol{u},\boldsymbol{u})]\ge|\boldsymbol{u}|_V^2-\|\!|\boldsymbol{B}_A|\!\|_\infty\,\|\boldsymbol{u}\|_H\,|\boldsymbol{u}|_V+\int_a^b\mathrm{Re}\left[\boldsymbol{u}^*\left(\boldsymbol{C}-\frac{1}{2}\boldsymbol{B}'\right)_S\boldsymbol{u}\right]dx. \tag{61}$$

Also, from Eq. (55)

$$\mathrm{Re}[p(\boldsymbol{u},\boldsymbol{u})]\ge|\boldsymbol{u}|_V^2-\|\!|\boldsymbol{B}_A|\!\|_\infty\,\|\boldsymbol{u}\|_H\,|\boldsymbol{u}|_V+\xi\,\|\boldsymbol{u}\|_H^2\,, \tag{62}$$

and by means of the arithmetic–geometric mean inequality (see Eq. (50))

$$\begin{aligned}\mathrm{Re}[p(\boldsymbol{u},\boldsymbol{u})] &\geq |\boldsymbol{u}|_V^2 - \|\boldsymbol{B}_A\|_\infty \left(\frac{\sigma}{2}\,\|\boldsymbol{u}\|_H^2 + \frac{1}{2\sigma}\,|\boldsymbol{u}|_V^2\right) + \xi\,\|\boldsymbol{u}\|_H^2 \\ &= \left(1 - \frac{1}{2\sigma}\|\boldsymbol{B}_A\|_\infty\right)|\boldsymbol{u}|_V^2 + \left(\xi - \|\boldsymbol{B}_A\|_\infty\frac{\sigma}{2}\right)\|\boldsymbol{u}\|_H^2 . \end{aligned} \tag{63}$$

For $2\sigma > \|\boldsymbol{B}_A\|_\infty$ we get

$$\mathrm{Re}[p(\boldsymbol{u},\boldsymbol{u})] \geq \left(1 - \frac{1}{2\sigma}\|\boldsymbol{B}_A\|_\infty\right)\|\boldsymbol{u}\|_V^2 + \left(\xi - 1 + \frac{1-\sigma^2}{2\sigma}\|\boldsymbol{B}_A\|_\infty\right)\|\boldsymbol{u}\|_H^2 \tag{64}$$

and the theorem is proved. □

We note here that a similar inequality may be proved by considering not only the skew-symmetric part of $\boldsymbol{B}$ and avoiding the use of Lemma 1. In that case, Eq. (55) is replaced by $\mathrm{Re}[\boldsymbol{u}^*\boldsymbol{C}_S\boldsymbol{u}] \geq \xi\boldsymbol{u}^*\boldsymbol{u}$ and the condition imposed on σ becomes $2\sigma > \|\boldsymbol{B}\|_\infty$. To proceed and in order to apply Lemma 2, the following result is needed.

Theorem 6. *Let* $\|\boldsymbol{T}_1\|_2 , \|\boldsymbol{T}_2\|_2 < \infty$. *Then,* $\boldsymbol{F} \in H, \forall \boldsymbol{w} \in V$.

Proof. The dual space of $H = \left[L^2(a,b)\right]^M$ is $H' \equiv H$. Since $\|\boldsymbol{T}_1\|_2 , \|\boldsymbol{T}_2\|_2 < \infty$ and $[a,b]$ is bounded, it is

$$\|\boldsymbol{F}\|_H \doteq \left(\int_a^b |\boldsymbol{C}\boldsymbol{F}_1 x + \boldsymbol{B}\boldsymbol{F}_1 + \boldsymbol{C}\boldsymbol{F}_2|^2\,dx\right)^{1/2} < \infty, \tag{65}$$

and the proof is completed. □

We now turn to the finite element approximation of solutions of variational problem (51). Let $V^h \subset V$ we consider the discrete variational problem: Find $\boldsymbol{u}_h \in V^h$ such that

$$\int_a^b \boldsymbol{w}_h^{*\prime}\boldsymbol{u}_h^{*\prime}dx + \int_a^b \boldsymbol{w}_h^*\boldsymbol{B}\boldsymbol{u}_h'dx + \int_a^b \boldsymbol{w}_h^*\boldsymbol{C}\boldsymbol{u}_h dx + \boldsymbol{w}_h^*(b)\boldsymbol{S}_2\boldsymbol{u}_h(b) - \boldsymbol{w}_h^*(a)\boldsymbol{S}_1\boldsymbol{u}_h(a) = \int_a^b \boldsymbol{w}_h^*\boldsymbol{F}dx, \quad \forall \boldsymbol{w}_h \in V^h. \tag{66}$$

The main result for the solution of problem (66) is stated in the following theorem.

Theorem 7. *Assume that for problem Eqs. (39)–(41) it is* $\|\boldsymbol{B}_A\|_\infty < 2\xi^{1/2}$. *Set* $\vartheta = \mathrm{K}_3/2$, $\mathrm{K}_3 = 1 - \frac{1}{2\sigma}\|\boldsymbol{B}_A\|_\infty$ *and select any value of* $\sigma \in \left(0.5\|\boldsymbol{B}_A\|_\infty, 0.5\|\boldsymbol{B}_A\|_\infty^{-1}J\right)$ *with* $J = 2\xi - 1 + \left((2\xi-1)^2 + 2\|\boldsymbol{B}_A\|_\infty^2\right)^{1/2}$. *Then, the error* $\boldsymbol{u} - \boldsymbol{u}_h$ *of the discrete approximation in problem (66) satisfies*

$$\|\boldsymbol{u} - \boldsymbol{u}_h\|_V \leq C \inf_{\boldsymbol{w}_h \in V^h} \|\boldsymbol{u} - \boldsymbol{w}_h\|_V , \tag{67}$$

where $C = 2\left(1 - \frac{1}{2\sigma}\|\boldsymbol{B}_A\|_\infty\right)^{-1}\left(1 + \|\boldsymbol{B}\|_\infty + \|\boldsymbol{C}\|_\infty + 2\|\boldsymbol{S}\|_\infty + \|\boldsymbol{S}'\|_\infty\right)$.

Proof. Since $\sigma > 0.5\|\boldsymbol{B}_A\|_\infty$ it is $\mathrm{K}_3 > 0$. Let $\vartheta = \mathrm{K}_3/2$ and the constant $c = \xi - 1 + \frac{1-\sigma^2}{2\sigma}\|\boldsymbol{B}_A\|_\infty$, defined by inequality (64). For Lemma 2 to apply with $\varphi = 0$, it must hold $c + \vartheta > 0$ and thus, $\|\boldsymbol{B}_A\|_\infty\sigma^2 - (2\xi-1)\,\sigma - \|\boldsymbol{B}_A\|_\infty/2 < 0$. It must therefore be $\sigma \in \left(0, 0.5\|\boldsymbol{B}_A\|_\infty^{-1}J\right)$. But since $\|\boldsymbol{B}_A\|_\infty < 2\xi^{1/2}$, it is always $0.5\|\boldsymbol{B}_A\|_\infty < 0.5\|\boldsymbol{B}_A\|_\infty^{-1}J$ and thus $\sigma \in \left(0.5\|\boldsymbol{B}_A\|_\infty, 0.5\|\boldsymbol{B}_A\|_\infty^{-1}J\right)$. Now, application of Lemma 2 with $\varphi = 0$ concludes the proof. □

For the approximation of the problem (66) by the Finite Element Method, we assume a partition of $[a,b]$ of the form $a = x_1 < x_2 < \cdots < x_{N+1} = b$ $N \in \mathbb{N}$. Let $P_\ell(z)$ be a polynomial of degree ℓ. We now set $V^h \doteq \{\mathbf{u}_h \in V : u_{hj}|_{[x_i,x_{i+1}]} \equiv P_\ell(x), i = 1,2,\ldots,N, j = 1,2,\ldots,N_m\}$. Obviously $V^h \subset V$. Assuming sufficient regularity of the exact solution, the use of Theorem 7 yields the standard Hilbert space error estimate (see, e.g., [38]), as follows

$$\|\boldsymbol{u} - \boldsymbol{u}_h\|_V \leq Ch^\ell\,\|\boldsymbol{u}\|_{\left[H^{\ell+1}(a,b)\right]^{Nm}} , \tag{68}$$

for some positive constant C.

In addition, an $\left[L^2(a,b)\right]^{N_m}$ error estimate is possible (see also [29]),

$$\|\boldsymbol{u} - \boldsymbol{u}_h\|_H \leq Ch^{\ell+1}\,\|\boldsymbol{u}\|_{\left[H^{\ell+1}(a,b)\right]^{Nm}} . \tag{69}$$

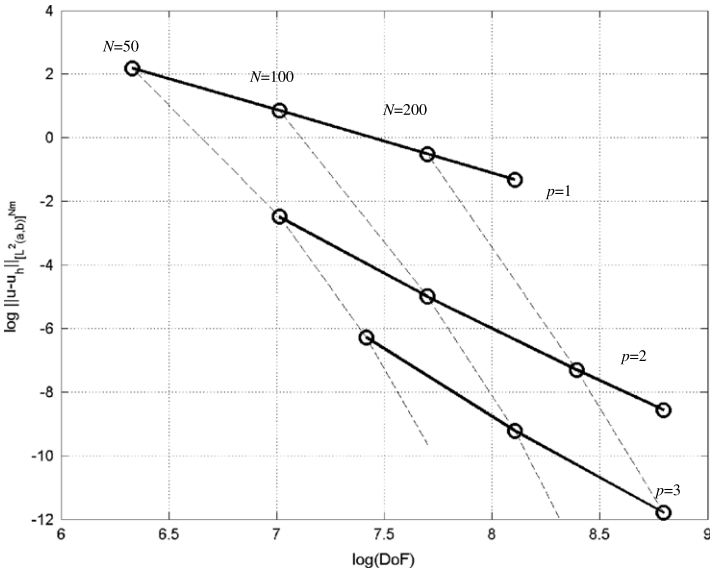

Fig. 9. L^2-error of the present CMS solution using $N_m = 11$ modes against DoF, in the case of the example of Fig. 2.

The above results will be confirmed with the aid of numerical experiments presented in the next section concerning acoustic propagation in inhomogeneous waveguides.

6. Numerical results and discussion

In this section calculations demonstrating the overall efficiency of the present method are shown and discussed. Also, numerical results are presented for the waveguide of Fig. 2 at higher frequency of excitation and for three-layered environments, illustrating the applicability of the methodology in more complex configurations. In all examined cases the local vertical basis $\{Z_n(z;x)\}$ and its derivatives, as well as the system coefficients a_{mn}, b_{mn} and c_{mn}, are numerically calculated through the solution of local VEP by application of the *hp*-FEM, as described in Section 4. Subsequently, the numerical solution of the CMS Eqs. (22), (25) is obtained by truncating the series (19) keeping a finite number of evanescent modes and discretizing the horizontal interval $a < x < b$ using the same uniform mesh for all modes. Thus the mesh size is $h = (b-a)/N$, where N denotes the number of elements, and the total degrees-of-freedom of the numerical scheme is given by $\mathrm{DoF} = (pN+1)\,N_m$, where N_m denotes the retained terms (modes) in the representation Eq. (19).

To begin with, we consider the underwater acoustic waveguide of Fig. 2 consisted of the water layer ($\rho_1 = 1\,\mathrm{g/cm^3}$, $c_1 = 1500\,\mathrm{m/s}$) and the sediment layer ($\rho_2 = 1.5\,\mathrm{g/cm^3}$, $c_2 = 1700\,\mathrm{m/s}$), terminated by the rigid bottom at a depth $H = 100\,\mathrm{m}$. The geometry of the internal interface $z = -h_1(x)$ and the upper surface $z = \eta(x)$ are kept the same as before, defined by Eqs. (26a) and (26b), respectively. Moreover, excitation by the first mode at frequency $f = 20\,\mathrm{Hz}$ is considered. In this case a reference (datum) solution has been obtained by the present method using $p = 6$ and $N = 300$ elements.

The convergence characteristics of the present method are plotted in Figs. 9 and 10. Fig. 9 is a log–log plot of the error calculated in the $\left[L^2(a,b)\right]^{N_m}$-norm, against the total DoF employed in the approximation. Solid lines correspond to interpolation polynomials of order $p = 1, 2, 3$. For all p the circle marks correspond to $N = 50, 100, 200$ elements, and for $p = 1, 2$ error data for $N = 300$ elements are also included. The estimated rates of the error decay for $p = 1, 2, 3$ are calculated to be 1.974, 3.124, 3.995, in compatibility with theoretical prediction by Eq. (68). The dashed lines are used to illustrate the *p*-convergence behavior. As expected for *p* convergence, these dashed curves present negative curvature. Small discrepancies from the theoretical estimates are attributed to the fact that a numerical result based on $p = 6$ has been used as the reference instead of the exact solution.

The corresponding error characteristics in the $\left[H^1(a,b)\right]^{N_m}$-norm are shown in Fig. 10. In this case, the observed rates for $p = 2, 3$ are calculated to be 2.28, 3.02, respectively, again in conformity with the theoretical prediction by Eq. (69), while an increased rate is obtained for $p = 1$, possibly due to pre-asymptotic behavior. As a useful remark, we obtain from the above figures that in the examined case, characterized by non-dimensional wavenumber $\kappa = 37$, quite accurate solutions are obtained by using approximately 1500DoF. Extensive numerical evidence from the above and cases of similar complexity has shown that $\mathrm{DoF}/\kappa \approx 50$, in this band of nondimensional wavenumbers, rendering the present method quite competitive from the point of view of computational efficiency.

A second example is presented in Fig. 11, where numerical results concerning the real part and the modulus of the calculated acoustic wave field are shown as obtained by present method, when the above waveguide is excited again by the first incident mode, but at higher frequency $f = 50\,\mathrm{Hz}$. In this case the characteristic nondimensional wavenumber is quite larger $\kappa \approx 93$ and the number of propagating modes is 6 both in the region of incidence and in the region of transmission.

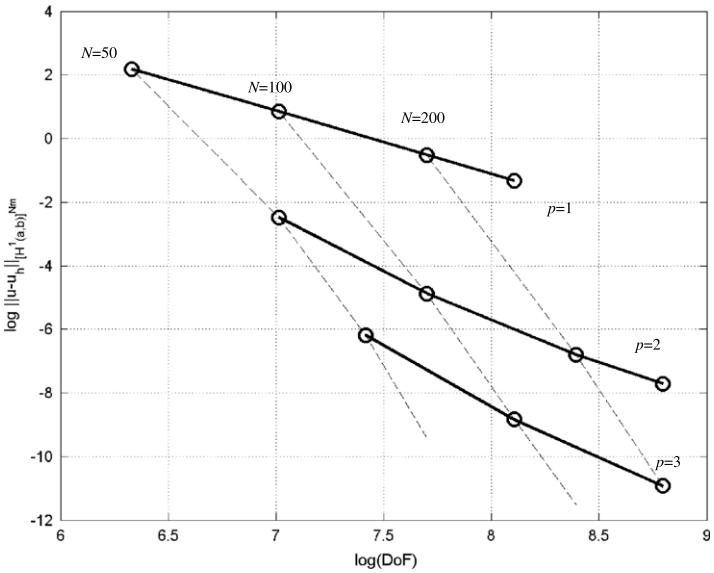

Fig. 10. H^1-error of the present CMS solution using $N_m = 11$ modes against DoF, in the case of the example of Fig. 2.

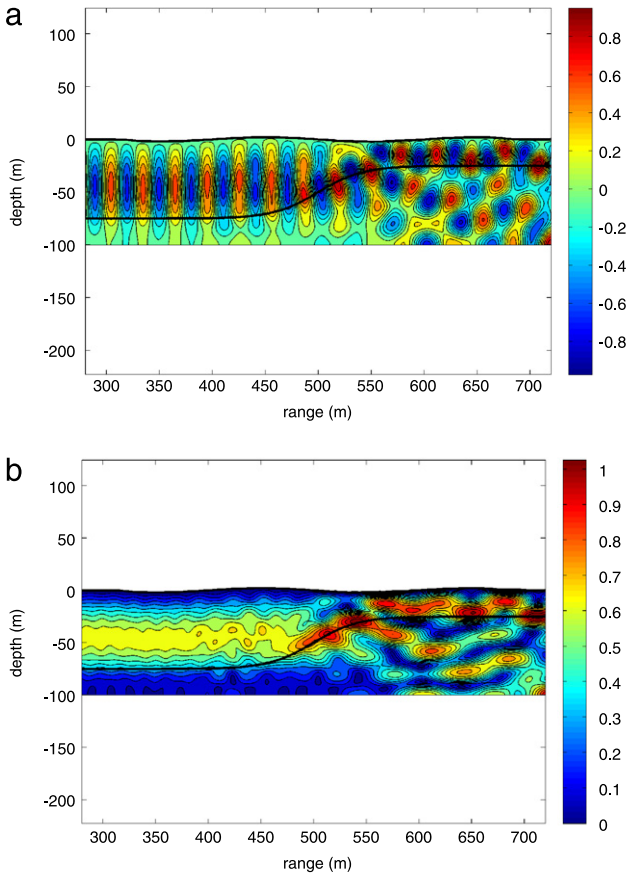

Fig. 11. Acoustic pressure in the waveguide of Fig. 2 as calculated by the present method, for excitation frequency 50 Hz and waveguide forcing by the first incident mode. (a) Real part and (b) modulus of the wave field.

This is a more computationally demanding problem compared to the previous one, since the acoustic pressure field becomes quite more oscillatory. The present local-mode series has been truncated by keeping 15 totally modes, including

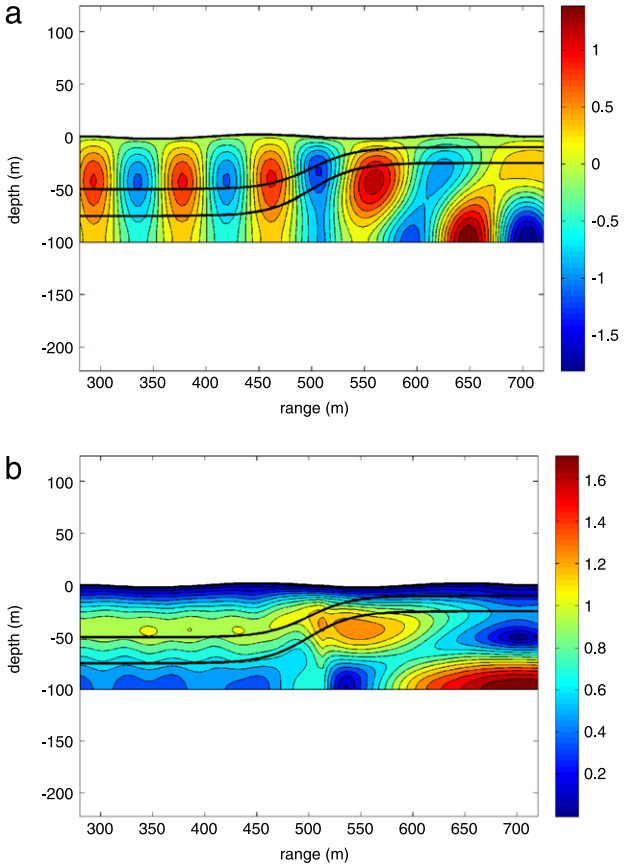

Fig. 12. Acoustic pressure in a three-layer waveguide as calculated by the present method. Excitation frequency 20 Hz and waveguide forcing by the first incident mode. Acoustic parameters: $\rho_1 = 1$ g/cm^3, $c_1 = 1500$ m/s, $\rho_2 = 1.5$ g/cm^3, $c_2 = 1700$ m/s, $\rho_3 = 1.7$ g/cm^3, $c_3 = 2000$ m/s. (a) Real part and (b) modulus of the wave field.

except of the propagating and the sloping-interface modes the first 8 evanescent modes. The coupled-mode system is discretized by using $N = 200$ elements based on uniform mesh and $p = 4$, which was proved to be enough for numerical accuracy.

As shown in Fig. 11 high-quality numerical solutions are obtained, keeping a small number of modes in the truncated local-mode series expansions and reducing the overall computational cost. To further illustrate this fact, a final example is presented in Fig. 12 corresponding to a more complicated environment resembling a three-layered ocean acoustic waveguide, terminated above by the free surface, $z = \eta(x)$ (which is again defined by Eq. (26b)), and below by a rigid flat horizontal bottom located at a depth $H = 100$ m. In this case the two interfaces separating the layers ($z = -h_1(x)$ and $z = -h_2(x)$) have similar shapes and are defined by formulas like Eq. (26a). In the examined case the water layer ($\rho_1 = 1$ g/cm^3, $c_1 = 1500$ m/s) and the first sediment layer ($\rho_2 = 1.5$ g/cm^3, $c_2 = 1700$ m/s) are overlying a heavier medium ($\rho_3 = 1.7$ g/cm^3, $c_3 = 2000$ m/s).

Numerical results concerning the real part of the calculated wave field, when the waveguide is excited at frequency $f = 20$ Hz and is again forced by the first incident mode are shown in Fig. 12(a), as calculated by the *hp*-FEM using 4th degree polynomials ($p = 4$). The corresponding acoustic pressure modulus $|p(x, z)|$ is plotted in Fig. 12(b). Again, the local-mode series is truncated by keeping 15 totally modes, and the coupled-mode system is discretized using $N = 200$ elements based on uniform horizontal mesh, the same for all modes $U_n(x)$, $n = -1, 0, 1, 2, \ldots$, which were proved to be enough for numerical convergence. Based on the above examples and extensive numerical evidence in similar cases we conclude that the present approach and numerical solution ensures the absolute and uniform convergence of the enhanced series and its derivatives, up to the boundaries, within each layer, providing useful results in the general multilayer case.

Taking into account that the various mode amplitudes $U_n(x)$ present different horizontal variability, a further improvement of the efficiency of the present *hp*-FEM is possible by using different horizontal meshes for different modes. Such an elaboration, in conjunction with grid adaptation techniques, based on information concerning the spatial variability of the system coefficients, and essentially the diagonal part of the matrices $\boldsymbol{B}$ and $\boldsymbol{C}$, will support the numerical treatment of complicated wave propagation and scattering problems in more demanding applications such as three-dimensional, multi-layered waveguides, and this is left to be examined in future work.

7. Conclusions

An improved coupled-mode method is presented for the efficient solution of the problem of time-harmonic wave propagation and scattering in non uniform stratified waveguides. The problem is governed by the Helmholtz equation with variable coefficients. Our method is based on an enhanced local-mode series for the representation of the wave field, including additional modes, which account for the effects of the inhomogeneous interfaces. Using the enhanced representation, in conjunction with an energy-type variational principle, a coupled-mode system of equations is derived for the determination of the unknown modal-amplitude functions. In the case of multilayered environments, h- and p-Finite Element Methods have been applied for the solution of both the local vertical eigenvalue problems and the resulting coupled mode system, exhibiting robustness and good rates of convergence. Numerical examples are presented in simple 2D acoustic propagation problems, illustrating the role and significance of the additional mode(s) and the overall efficiency of the present model, that can be naturally extended to treat propagation and scattering problems in more general waveguides.

Appendix A

In the case of homogeneous two-layer waveguide, with constant physical properties ρ_1, c_1 and ρ_2, c_2, the exact analytical solution of the vertical eigenvalue problem is given as follows (see also [2])

$$Z_n(z) = \begin{cases} b_1^n \sin\left(\sqrt{k_1^2-\lambda_n^2}(z-\eta)\right), & \eta \geq z \geq -h_1 \\ b_2^n \cos\left(\sqrt{k_2^2-\lambda_n^2}(z+H)\right), & -h_1 \geq z \geq -H \end{cases}, \tag{A.1}$$

where

$$b_2^n = -b_1^n \frac{\sin\left(\sqrt{k_1^2-\lambda_n^2}(h_1+\eta)\right)}{\cos\left(\sqrt{k_2^2-\lambda_n^2}(H-h_1)\right)}, \quad n = 1, 2, \ldots. \tag{A.2}$$

In this case, the eigenvalues λ_n are found as the roots of the equation

$$\begin{aligned} &\frac{\rho_2}{\rho_1}\frac{\sqrt{k_1^2-\lambda_n^2}}{\sqrt{k_2^2-\lambda_n^2}} \cos\left(\sqrt{k_1^2-\lambda_n^2}(\eta+h_1)\right)\cos\left(\sqrt{k_2^2-\lambda_n^2}(H-h_1)\right) \\ &\quad = \sin\left(\sqrt{k_1^2-\lambda_n^2}(\eta+h_1)\right)\sin\left(\sqrt{k_2^2-\lambda_n^2}(H-h_1)\right), \end{aligned} \tag{A.3}$$

which expresses the continuity of $\rho^{-1}\partial Z/\partial z$ across the interface at $z = -h_1$. The remaining constants b_1^n, $n = 1, 2, \ldots$, of the above solution are fixed by normalization.

Appendix B

For the detailed proof of Theorem 4 we consider the following inequality concerning the sesquilinear form $p(\cdot,\cdot) : V \times V \to \mathbb{C}$, which is defined by Eq. (52),

$$\begin{aligned} |p(\boldsymbol{w},\boldsymbol{u})| &\leq \left|\int_a^b \boldsymbol{w}^{*\prime}\boldsymbol{u}'dx\right| + \left|\int_a^b \boldsymbol{w}^*\boldsymbol{B}\boldsymbol{u}'dx\right| + \left|\int_a^b \boldsymbol{w}^*\boldsymbol{C}\boldsymbol{u}dx\right| + \left|\boldsymbol{w}^*(b)\boldsymbol{S_2}\boldsymbol{u}(b) - \boldsymbol{w}^*(a)\boldsymbol{S_1}\boldsymbol{u}(a)\right| \\ &\leq \int_a^b \left|\boldsymbol{w}^{*\prime}\boldsymbol{u}'\right|dx + \int_a^b \left|\boldsymbol{w}^*\boldsymbol{C}\boldsymbol{u}\right|dx + \int_a^b \left|\boldsymbol{w}^*\boldsymbol{B}\boldsymbol{u}'\right|dx + \left|\boldsymbol{w}^*(b)\boldsymbol{S_2}\boldsymbol{u}(b) - \boldsymbol{w}^*(a)\boldsymbol{S_1}\boldsymbol{u}(a)\right|. \end{aligned} \tag{B.1}$$

Using assumption (A2) in the above and applying the Cauchy–Schwarz inequality we obtain

$$\begin{aligned} |p(\boldsymbol{w},\boldsymbol{u})| \leq{}& \left(\int_a^b \left|\boldsymbol{w}^{*\prime}\right|^2 dx\right)^{\frac{1}{2}}\left(\int_a^b \left|\boldsymbol{u}'\right|^2 dx\right)^{\frac{1}{2}} + \left(\int_a^b \left|\boldsymbol{w}^*\right|^2 dx\right)^{\frac{1}{2}}\left(\int_a^b \left|\boldsymbol{B}\boldsymbol{u}'\right|^2 dx\right)^{\frac{1}{2}} \\ &+ \left(\int_a^b \left|\boldsymbol{w}^*\right|^2 dx\right)^{\frac{1}{2}}\left(\int_a^b |\boldsymbol{C}\boldsymbol{u}|^2 dx\right)^{\frac{1}{2}} + \left(\int_a^b \left|\boldsymbol{w}^{*\prime}\right|^2 dx\right)^{\frac{1}{2}}\left(\int_a^b |\boldsymbol{S}\boldsymbol{u}|^2 dx\right)^{\frac{1}{2}} \\ &+ \left(\int_a^b \left|\boldsymbol{w}^*\right|^2 dx\right)^{\frac{1}{2}}\left(\int_a^b \left|\boldsymbol{S}'\boldsymbol{u}\right|^2 dx\right)^{\frac{1}{2}} + \left(\int_a^b \left|\boldsymbol{w}^*\right|^2 dx\right)^{\frac{1}{2}}\left(\int_a^b \left|\boldsymbol{S}\boldsymbol{u}'\right|^2 dx\right)^{\frac{1}{2}}. \end{aligned} \tag{B.2}$$

For every matrix $\boldsymbol{A} \in \mathbb{M}_{N_m \times N_m}$ and vector $\boldsymbol{y} \in \mathbb{C}^{N_m}$ it holds $|\boldsymbol{Ay}|^2 \equiv \boldsymbol{y}^* \boldsymbol{A}^* \boldsymbol{Ay} \equiv \|\boldsymbol{Ay}\|_2^2 \leq \|\boldsymbol{A}\|_2^2 |\boldsymbol{y}|^2$. Using the latter inequality in (B.2) and assumptions (A1) and (A2)

$$
\begin{aligned}
|p(\boldsymbol{w}, \boldsymbol{u})| \leq & \left(\int_a^b \left| \boldsymbol{w}^{*\prime} \right|^2 dx \right)^{\frac{1}{2}} \left(\int_a^b \left| \boldsymbol{u}' \right|^2 dx \right)^{\frac{1}{2}} + \|\!| \boldsymbol{B} |\!\|_\infty \left(\int_a^b \left| \boldsymbol{w}^* \right|^2 dx \right)^{\frac{1}{2}} \left(\int_a^b \left| \boldsymbol{u}' \right|^2 dx \right)^{\frac{1}{2}} \\
& + \|\!| \boldsymbol{C} |\!\|_\infty \left(\int_a^b \left| \boldsymbol{w}^* \right|^2 dx \right)^{\frac{1}{2}} \left(\int_a^b |\boldsymbol{u}|^2 dx \right)^{\frac{1}{2}} + \|\!| \boldsymbol{S} |\!\|_\infty \left(\int_a^b \left| \boldsymbol{w}^{*\prime} \right|^2 dx \right)^{\frac{1}{2}} \left(\int_a^b |\boldsymbol{u}|^2 dx \right)^{\frac{1}{2}} \\
& + \|\!| \boldsymbol{S}' |\!\|_\infty \left(\int_a^b \left| \boldsymbol{w}^* \right|^2 dx \right)^{\frac{1}{2}} \left(\int_a^b |\boldsymbol{u}|^2 dx \right)^{\frac{1}{2}} + \|\!| \boldsymbol{S} |\!\|_\infty \left(\int_a^b \left| \boldsymbol{w}^* \right|^2 dx \right)^{\frac{1}{2}} \left(\int_a^b \left| \boldsymbol{u}' \right|^2 dx \right)^{\frac{1}{2}}, \qquad \text{(B.3)}
\end{aligned}
$$

where the notation $\|\!| \boldsymbol{Q} |\!\|_\infty = ess\ sup_{x \in [a,b]} \{ \| \boldsymbol{Q} \|_2 \}$ has been used. Since $\|\boldsymbol{w}^*\|_V = \|\boldsymbol{w}\|_V$ we finally have

$$
|p(\boldsymbol{w}, \boldsymbol{u})| \leq \mathrm{K}_2 \|\boldsymbol{u}\|_V \|\boldsymbol{w}\|_V, \quad \text{where } \mathrm{K}_2 = 1 + \|\!| \boldsymbol{B} |\!\|_\infty + \|\!| \boldsymbol{C} |\!\|_\infty + 2\|\!| \boldsymbol{S} |\!\|_\infty + \|\!| \boldsymbol{S}' |\!\|_\infty. \qquad \text{(B.4)}
$$

References

[1] L.M. Brekhovskikh, O. Godin, Acoustics of layered media, I: plane and quasi-plane waves, II: point sources and bounded beams, in: Springer Series on Wave Phenomena, 1999.
[2] C.A. Boyles, Acoustic waveguides, in: Applications to Ocean Science, J. Wiley & Sons, 1984.
[3] F. Jensen, W. Kupperman, M. Porter, H. Schmidt, Computational Ocean Acoustics, AIP Press, 1994.
[4] E.M. Salomons, Computational Atmospheric Acoustics, Kluwer Academic Publishers, Dordrecht, 2001.
[5] B.Z. Katsenelenbaum, L. Mercader del Rio, M. Pereyaslavets, M. Sorolla Ayza, M. Thumm, Theory of Nonuniform Waveguides, The Cross-Section Method, IEE London, 1998.
[6] D. Lee, M.H. Schultz, Numerical Ocean Acoustic Propagation in Three Dimensions, World Scientific, Singapore, 1995.
[7] T. Belytschko, Y. Krongauz, D. Organ, M. Fleming, P. Krysl, Meshless methods: an overview and recent developments, Comput. Methods Appl. Mech. Engrg. 139 (1996) 3–47.
[8] B.T. Jin, Y. Zheng, A meshless method for some inverse problems associated with the Helmholtz equation, Comput. Methods Appl. Mech. Engrg. 195 (2006) 2270–2288.
[9] N. Biggs, Wave trapping in a two-dimensional sound-soft or sound-hard acoustic waveguide of slowly-varying width, Wave Motion 49 (2012) 24–33.
[10] A.F. Smith, N.C. Ovende, R.I. Bowles, Flow and geometry induced scattering of high frequency acoustic duct modes, Wave Motion 49 (2012) 109–124.
[11] S. Grilli, T. Pedersen, P. Stephanisen, A hybrid boundary element method for shallow acoustic propagation over an irregular bottom, Eng. Anal. Bound. Elem. 21 (1998) 131–145.
[12] R.B. Evans, A coupled mode solution for the acoustic propagation in a waveguide with stepwise depth variations of a penetrable bottom, J. Acoust. Soc. Am. 74 (1983) 188–195.
[13] R.B. Evans, The decoupling of stepwise coupled modes, J. Acoust. Soc. Am. 80 (5) (1986) 1414–1418.
[14] F.B. Jensen, On the use of stair steps to approximate bathymetry changes in ocean acoustic models, J. Acoust. Soc. Am. 104 (3) (1998) 1310–1315.
[15] W. Luo, R. Zhang, H. Schmidt, An efficient and numerically stable coupled-mode solution for range-dependent propagation, J. Comp. Acous. 20 (2012) 1250008.
[16] J.A. Fawcett, A derivation of the differential equations of coupled mode propagation, J. Acoust. Soc. Am. 97 (1992) 290–295.
[17] O.A. Godin, A note on differential equations of coupled mode propagation in fluids, J. Acoust. Soc. Am. 103 (1) (1998) 159–168.
[18] G.A. Athanassoulis, K.A. Belibassakis, A consistent coupled-mode theory for the propagation of small-amplitude water waves over variable bathymetry regions, J. Fluid Mech. 389 (1999) 275–301.
[19] G.A. Athanassoulis, K.A. Belibassakis, D.A. Mitsoudis, N.A. Kampanis, V.A. Dougalis, Coupled-mode and finite-element solutions of underwater sound propagation problems in stratified acoustic environments, J. Comput. Acoust. 16 (1) (2008) 83–116.
[20] G.A. Athanassoulis, K.A. Belibassakis, Rapidly-convergent local-mode representations for wave propagation and scattering in curved-boundary waveguides, in: Proc. 6th Int. Conference on Mathematical and Numerical Aspects of Wave Propagation, Finland, 2003.
[21] C. Hazard, E. Lunéville, An improved multimodal approach for non-uniform acoustic waveguides, IMA J. Appl. Math. 73 (4) (2008) 668–690.
[22] J.F. Mercier, A. Maurel, Acoustic propagation in non uniform waveguides: revisiting Webster equation using evanescent boundary modes, Proc. R. Soc. A 469 (2156) (2013) 20130186.
[23] K.A. Belibassakis, G.A. Athanassoulis, Th. Gerostathis, A coupled-mode model for the refraction–diffraction of linear waves over steep three-dimensional bathymetry, Appl. Ocean Res. 23 (2001) 319–336.
[24] K.A. Belibassakis, G.A. Athanassoulis, Three-dimensional Green's function of harmonic water-waves over a bottom topography with different depths at infinity, J. Fluid Mech. 510 (2004) 267–302.
[25] K.A. Belibassakis, G.A. Athanassoulis, Extension of second-order Stokes theory to variable bathymetry, J. Fluid Mech. 464 (2002) 35–80.
[26] K.A. Belibassakis, G.A. Athanassoulis, A coupled-mode system with application to nonlinear water waves propagating in finite water depth and in variable bathymetry regions, Coastal Eng. 58 (2011) 337–350.
[27] K.A. Belibassakis, A boundary element method for the hydrodynamic analysis of floating bodies in general bathymetry regions, Eng. Anal. Bound. Elem. 32 (2008) 796–810.
[28] K.A. Belibassakis, G.A. Athanassoulis, A coupled-mode model for the hydroelastic analysis of large floating bodies over variable bathymetry regions, J. Fluid Mech. 531 (2005) 221–249.
[29] T.J.R. Hughes, The Finite Element Method, Linear Static and Dynamic Finite Element Analysis, Dover Publications Inc., 1987.
[30] A. Maurel, J.-F. Mercier, S. Félix, Wave propagation through penetrable scatterers in a waveguide and through a penetrable grating, J. Acoust. Soc. Am. 135 (1) (2014) 165–174.
[31] E. Coddington, N. Levinson, Theory of Ordinary Differential Equations, McGraw Hill, New York, 1955.
[32] E.G. Tichmarsh, Eigenfunction Expansions, Calderon Press, 1962.
[33] G. Frisk, Ocean and seabed acoustics, in: A Theory of Wave Propagation, Prentice Hall, 1994.
[34] L.B. Felsen, N. Marcuvitz, Radiation and Scattering of Waves, Prentice Hall, Englewood Cliffs, New Jersey, 1973.
[35] G. Strang, G.J. Fix, An Analysis of the Finite Element Method, Englewood Cliffs, NJ Prentice-Hall, 1973.
[36] R.A. Adams, Sobolev Spaces, Academic Press, 1975.
[37] M. Miklavčič, Applied Functional Analysis and Partial Differential Equations, World Scientific Publishing, Singapore, 2001.
[38] I. Babuška, M. Suri, The p- and h–p-versions of the finite element method, an overview, Comput. Methods Appl. Mech. Engrg. 80 (1–3) (1990) 5–26.